UNIVERSITY OF SÃO PAULO FFCLRP –

DEPARTMENT OF PHYSICS

Postgraduate in Applied Physics to Medicine and Biology

JEFERSON DA SILVA OLIVEIRA

Multitherapeutic Nanoplatform Based on Scintillating Anthracene, Silver@Antracene, and Gold@Anthracene Nanoparticles for Combined Radiation and Photodynamic Therapies: Enhancing Radiation Dose while Generating, Trapping, Probing, or Delivering Singlet Oxygen Species

Nanoplataforma terapêutica baseada em nanopartículas cintiladoras de Antraceno, Prata@Antraceno e Ouro@Antraceno para Combinação de Radioterapia e Terapia Fotodinâminca: Aumento de dose de radiação, geração, aprisionamento, detecção ou liberação de Oxigênio Singleto.

Ribeirão Preto – SP

2021

JEFERSON DA SILVA OLIVEIRA

Multitherapeutic Nanoplatform Based on Scintillating Anthracene, Silver@Antracene, and Gold@Anthracene Nanoparticles for Combined Radiation and Photodynamic Therapies: Enhancing Radiation Dose while Generating, Trapping, Probing, or Delivering Singlet Oxygen Species

Nanoplataforma terapêutica baseada em nanopartículas cintiladoras de Antraceno, Prata@Antraceno e Ouro@Antraceno para Combinação de Radioterapia e Terapia Fotodinâminca: Aumento de dose de radiação, geração, aprisionamento, detecção ou liberação de Oxigênio Singleto.

Dissertation presented to Faculty of Philosophy, Sciences and Literature of the University of São Paulo, as part of the requirements for acquirement the grade of Master of Sciences.

Concentration area: Applied Physics to Medicine and Biology.

Advisor: Prof. Dr. Éder José Guidelli

Ribeirão Preto – SP
2021

FICHA CATALOGRÁFICA

Serviço de Documentação da Universidade de São Paulo Faculdade de Filosofia, Ciências e Letras de Ribeirão Preto

Jeferson da Silva Oliveira

Multitherapeutic Nanoplatform Based on Scintillating Anthracene, Silver@Antracene, and Gold@Anthracene Nanoparticles for Combined Radiation and Photodynamic Therapies: Enhancing Radiation Dose while Generating, Trapping, Probing, or Delivering Singlet Oxygen Species / Jeferson da Silva Oliveira; Orientador: Prof. Dr. Éder José Guidelli.

Ribeirão Preto - SP, 2020.

Dissertation (M.Sc. - Postgraduate Program in Applied Physics to Medicine and Biology) - Faculty of Philosophy, Sciences and Literature of the University of São Paulo, 2021.

1. Nanoparticle. 2. Radiation Therapy 3. Photodynamic Therapy 4. Cancer 5.Plasmon-enhanced fluorescence

Name: Jeferson da Silva Oliveira

Title: Multitherapeutic Nanoplatform Based on Scintillating Anthracene, Silver@Antracene, and Gold@Anthracene Nanoparticles for Combined Radiation and Photodynamic Therapies: Enhancing Radiation Dose while Generating, Trapping, Probing, or Delivering Singlet Oxygen Species

Título: Nanoplataforma terapêutica baseada em nanopartículas cintiladoras de Antraceno, Prata@Antraceno e Ouro@Antraceno para Combinação de Radioterapia e Terapia Fotodinâminca: Aumento de dose de radiação, geração, aprisionamento, detecção ou liberação de Oxigênio Singleto.

Dissertation presented to Faculty of Philosophy, Sciences and Literature of the University of São Paulo, as part of the requirements for acquirement the grade of Master of Sciences.

Approved in:

Examination Board

Prof. Dr. _____

Institution: _____

Judgment: _____

Prof. Dr. _____

Institution: _____

Judgment: _____

Prof. Dr. _____

Institution: _____

Judgment: _____

I dedicate this work to my family

AKNOWLEDGMENTS

First, I would like to thank God for life, intelligence and health. All of this work is thanking Him. I want to express my deep gratitude to all of my family that always supported me, love and encouragement, not only with my education but in all aspects of my life specially my father, my mother and my brother. My thanks to my aunt Marlene and family that always helped and motivated to go ahead,

I would like to thank my advisor, Éder José guidelli for his advices, help, collaboration and his caring about many aspects to my life. I learned many things with him and all the time that I need his knowledge he was available. Thanks so much. My gratitude to professor Dr. Oswaldo Baffa for the suggestions and collaboration in this work and my gratitude to professor Dr. Iuri Borissevitch for the donation of porphyrin and his suggestions.

My special and sincere thanks to my colleague, Milene and Mariana, for his untiring supports and suggestions in my work whenever I need their help.

Many thanks to colleagues Iara, Sudi, Seti, Cleiton, Thirupaty, Emanuel Daniele, Luismar for the partnership and for providing a good working environment and collaboration even in different research groups. My special gratitude to Iara for introducing me to nanodose and new coworkers. My gratitude to my colleagues who lived with me at USP for the moments together and supporting when I need some help.

I would like to thank specially Professor Dra Ana Paula Ramos for supporting, suggestions and classes during this master. Her collaboration is so important to this work. Furthermore, my gratitude to Professor Dra Patricia Nicolucci for partnership in other works related to graduation and for motivation in my work.

My gratitude to Nilza to her hard work always helping me and all of the students that need some help about graduation and thanks to all of the technician helping me specially Carlos and Eldereis. Their contribution were so important to experimental stage of this work.

Lastly, my gratitude to all employers of USP for supporting me and all my research group with their good and hard work so that research activities could move forward.

Jeferson da Silva Oliveira

RESUMO

Jeferson da Silva Oliveira. **Nanoplataforma terapêutica baseada em nanopartículas cintiladoras de Antraceno, Prata@Antraceno e Ouro@Antraceno para Combinação de Radioterapia e Terapia Fotodinâminca: Aumento de dose de radiação, geração, aprisionamento, detecção ou liberação de Oxigênio Singleto.** 2021. Dissertação (Mestrado – Programa de Pós- Graduação em Física Aplicada à Medicina e Biologia) - Departamento de Física da Faculdade de Filosofia, Ciências e Letras de Ribeirão Preto, Universidade de São Paulo, Ribeirão Preto; 2021.

Nanopartículas de antraceno e nanopartículas metálicas revestidas com antraceno (metal@antraceno) foram sintetizadas e utilizadas como uma nanoplataforma com o objetivo de combinar radioterapia e terapia fotodinâmica. A síntese de nanopartículas de antraceno na presença de prata ou ouro coloidal provocou a redução do raio hidrodinâmico de acordo com a concentração das nanopartículas metálicas indicando a formação de nanoestruturas *core-shell*, conforme revelado por AFM e DLS. Além do tamanho reduzido, as nanopartículas *core-shell* apresentaram maior emissão fluorescente. Foi identificado maior aumento para Ag@antraceno em comprimentos de onda que se aproximam do pico de ressonância plasmônica, sugerindo aumento por acoplamento plasmônico. O aumento luminescente dependente do tamanho das nanopartículas e da distância entre o núcleo de metal e a área de superfície das nanopartículas resultou em um diâmetro ideal entre 100 nm e 150 nm. Foi investigada também a geração de oxigênio singlete ($^1O_2$) por espectroscopia de ressonância de spin eletrônico (ESR) utilizando marcador de spin (*spin-trap)* e por espectroscopia de fluorescência. Os resultados de ESR/spin-trap revelaram que, na presença de porfirina, tanto as nanopartículas de antraceno quanto as *core-shell* atuaram como mediadores de energia para a geração de $^1O_2$ sob exposição luminosa. Experimentos de supressão de fluorescência mostraram que as nanopartículas *core-shell* capturam $^1O_2$ em taxas mais altas por apresentarem menores tamanhos e maiores áreas superficiais do que as nanopartículas de antraceno. Juntos, os resultados de ESR e fluorescência sugeriram que a produção global de $^1O_2$ ($^1O_2$ capturado por spin-trap + $^1O_2$ capturado por moléculas de antraceno na superfície) foi maior para as nanopartículas core-shell do que para as nanopartículas de antraceno. Além disso, devido ao fenômeno de aumento fluorescente por acoplamento plasmônico e à maior área superficial, as nanopartículas de Ag@Ant se destacaram como uma nova e mais sensível sonda fluorescente para $^1O_2$. Durante a irradiação com raios-X, as nanopartículas de antraceno e Ag@Ant aprisionaram $^1O_2$; proporcionando posteriormente a liberação sustentada do mesmo por até 12 dias após a irradiação. Esta pode ser uma

estratégia interessante para estender o tratamento radioterápico após as sessões de irradiação. Além disso, a presença da nanopartícula metálica no núcleo da nanoestrutura *core-shell* aumentou a interação com os raios X, aumentando a dose de radiação ao redor da nanopartícula. Portanto, as nanoestruturas de metal@antraceno se destacam como potenciais candidatas no tratamento do câncer por diferentes abordagens, a depender da configuração da nanopartícula.
Palavras Chave: Nanopartículas, Raditerapia, Terapia Fotodinâmica, Câncer, Aumento Fluorescente por acoplamento plasmônico.

ABSTRACT

Jeferson da Silva Oliveira. **Multitherapeutic Nanoplatform Based on Scintillating Anthracene, Silver@Antracene, and Gold@Anthracene Nanoparticles for Combined Radiation and Photodynamic Therapies: Enhancing Radiation Dose while Generating, Trapping, Probing, or Delivering Singlet Oxygen Species** 2021. Dissertation (M.Sc. - Postgraduate Program in Applied Physics to Medicine and Biology) - Faculty of Philosophy, Sciences and Literature, University of São Paulo, Ribeirão Preto - SP, 2021.

We have synthesized anthracene and metal@anthracene core-shell nanoparticles and propose that they be used as a nanoplatform that combines radiation and photodynamic therapies. Synthesis of anthracene nanoparticles in the presence of colloidal silver or gold reduced the hydrodynamic radius in a concentration-dependent manner and caused core-shell nanostructures to grow, as revealed by AFM and DLS. Besides reduced size, the core-shell nanoparticles presented enhanced fluorescence emission. Fluorescence enhancements were higher for Ag@anthracene nanoparticles and for wavelengths approaching the plasmon resonance peak, which suggested a plasmon-enhancement phenomenon. The size-dependent enhancement in fluorescence associated with the distance between the metal core and the surface area of the nanoparticles provided an optimal core-shell diameter of 100–150 nm. We investigated singlet oxygen ($^1O_2$) generation by electron spin resonance spectroscopy (ESR) with a spin-trap and by fluorescence spectroscopy. The ESR/spin-trap results revealed that, in the presence of a porphyrin, anthracene nanoparticles and the core-shell nanoparticles acted as energy mediators for $^1O_2$ generation under exposure to light. Fluorescence suppression experiments showed that the core-shell nanoparticles captured $^1O_2$ at higher rates because they presented smaller size and larger surface area than anthracene nanoparticles. Together, the ESR and fluorescence results suggested that overall production of $^1O_2$ ($^1O_2$ captured by spin-trap + $^1O_2$ captured by surface anthracene molecules) was higher for the core-shell nanoparticles than for anthracene nanoparticles. Moreover, because of plasmon-enhanced fluorescence and larger surface area, the Ag@anthracene nanoparticles stood out as a new and more sensitive fluorescent probe for $^1O_2$. During irradiation with X-rays, both anthracene and Ag@anthracene nanoparticles trapped $^1O_2$; subsequently, they afforded sustained release of the trapped $^1O_2$ for up 12 days after irradiation. This could be an interesting strategy to extend the radiation therapy treatment after the irradiation sessions. Furthermore, the presence of the metallic nanoparticle in the core of the core-shell nanostructure increased interaction with X-rays, raising the radiation dose around

the nanoparticle. Therefore, metal@anthracene nanostructures may allow cancer treatment by different approaches depending on nanoparticle configuration.
Keywords: Nanoparticle, Radiation Therapy, Photodynamic Therapy, Cancer, Plasmon-enhanced fluorescence

LIST OF FIGURES

Table of contents

1. Introduction

The development of the nanotechnology researches are growing extensively due to its applicability in several knowledge fields, affording relations in the interface of the chemistry, physics and biology[1]. In this sense, nanotechnology has been inserted in the context of a Third Wave of Technological Innovation. The first Wave happened with the advent of the steam engine, the mechanization of the textile industry, the manipulation of cast iron and other innovations. Such transformations brought several changes in social relations and the construction of a new reality.[2]

The Second Wave of the technology innovation occurred with scientific-technology development characterized by several discoveries such as electric power, telephone, and motor burning, leading to changes in the perceptions of social relations and work[2]. Lastly, the third Wave of the innovation is characterized by several discoveries in the informatic field, biotechnology, new materials, and nanotechnology, that is one of the main advances of the technology innovation.[2] Thus, nanotechnology researches have been widely developed in several areas of the human life as engineering, biology, physics, chemistry, medical diagnostics and treatment. For biomedical applications, nanodevices are useful for drug delivery systems, to enhance biocompatibility besides improving pharmacokinetics of therapeutics and nanotherapeutics agents.[3]

One of the advantages of the nanoscale manipulation is that the material can acquire some features or even improving its characteristics increasing efficiency of some chemical, physical or biological process. Metal nanoparticles, for instance, can be used to enhance the power conversion efficiency of the solar cells.[4,5] Another relevant area is environment, in which nanotechnology has been used in green water treatment to remove pesticides, pathogens, and heavy metals, improving the water quality.[6,7]

Once the optics, magnetics, and electronics properties depend of the size and shape of the nanomaterial[8], it is possible to synthesize materials with specific features for biomedical application such as biological sensors, diseases treatment, medical imaging. In this sense, more sensitive detectors and nanodevices have been developed allowing both early diagnosis and diseases treatments. Gold nanoparticles, for instance, have been widely used for molecular image, drug delivery, therapy and diagnosis.[3]

In addition to improve diagnostics, development of nanodevices for cancer treatment have been received special attention recently due to the high incidence of this disease. According to the American Cancer Society (ACS), in 2020 1,806,590 new cancer cases and 606,530 cancer deaths are expected in United States, [9] while in Brazil 582,590 new cancer cases are expected, with prostate and female breast

the most common cases of this disease.[10] Furthermore, is reported that researches in nanomedicine have been performed with focus on diagnostics and medical devices, mainly for earlier disease detection of tumor of brain, lung, muscle, and liver[11] which become relevant researches for a new cancer treatment approaches.

The traditional and widely used therapy for cancer is Radiotherapy (RT) and chemotherapy. However, both display side effects as high recurrence rate and cumulative doses respectively, besides reducing life quality in many cases. [10,12] Recent studies report gastrointestinal side effects for chemotherapy leading to anorexia, weight loss, anemia, fatigue among others[13] whereas radiotherapy, although decreases mortality risk for breast cancer, can cause heart disease or even another cancer later.[14]

In this context, Photodynamic Therapy (PDT) is an alternative method for cancer treatment for being a noninvasive technique allowing better control in terms of local administration of energy/drug, improving the patient's life quality and leading to successful treatment outcomes.[12,15,16] For this reason, it has been applied in several clinical treatments such as esophageal, bladder, and head and neck cancers.[17] In addition to kill cancer cell, another advantage of this therapy is the use of the light for photo stimulation, i.e., the healthy cells around some lesions are stimulated to heal due to interactions between the light and some compounds present in the cells such as lipids, proteins, and nucleic acids.[18]

Once the objective of this work is the synthesis and characterization of nanodevices in the context of new approaches for cancer treatments employing RT and PDT it is important to discuss more deeply some theoretical fundaments (like fluorescence, radioluminescence, Metal Enhanced Fluorescence, among others) that will be made in follow section.

2. Theoretical Fundaments

2.1 Photodynamic Therapy (PDT)

The PDT treatment is based on controlled and localized irradiation of a photosensitizer (PS) with UV-vis light in a specific wavelength range, to result in light absorption and consequent generation of Reactive Oxygen Species (ROS) like singlet oxygen ($^1O_2$), which is the most toxic ROS.[12,19,20] The photooxidation may occur by two mechanisms: (i) electron transfer between PS in excited state (PS*) and some substance in medium to form radicals and hence interact with molecular oxygen leading to ROS and (ii) the PS* transfer energy to molecular oxygen in the environment leading to a change from triplet to singlet oxygen state generating $^1O_2$ species[16,19] as can be seen in Fig.1. These reactive species act causing cellular damage, killing tumor cells or even acting indirectly leading a vascular damage.[12] In this sense, $^1O_2$ play as stronger cytotoxic agent once react faster with several compounds in biological environment besides having localized action due its lower diffusion, once its lifetime is short, causing damage in regions close to the PS*.[21] The vessels damage due to oxidative processes after PDT sessions can lead hypoxia (lack of oxygen) and hence tumor death.[22]

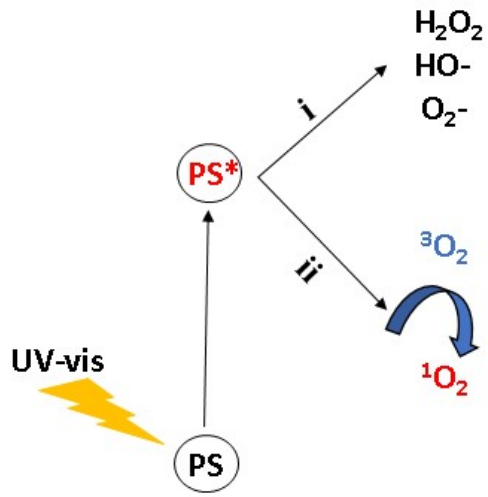

Figure 1 - Mechanisms of the ROS generation: i electron transfer between PS* and compounds in the medium; ii energy transfer from PS* and molecular oxygen

As can be seen, PSs play an important role since they act as energy intermediates in the PDT treatment. To be considered as a good PS it is required to present low toxicity in absence of light, high affinity and penetration on the sick tissue, biocompatibility, suitable photo-physical properties, among others.[18] According to the literature, the suitable absorption wavelength range for a PS is between 600 – 750nm[18] due to the higher penetration of light in biological tissues (between 1 – 6 mm).[18] Considering

the photophysical properties of molecules, porphyrins, chlorines, and phthalocyanines are the main compounds considered in PDT .[18]

Chlorines are chlorophyll derivates that display absorption in the therapeutic window (630 – 680 nm) standing as good candidates for PDT treatment. Although the chlorines display high absorption in infra-red region that in turn can be used for deeper cancer treatment, chlorines synthesis are expensive, and complex purification processes are required.[18]

Another good candidate is phthalocyanines that are dyes widely used in textile industry also showing high absorption in the infra-red range. Some phthalocyanines have higher absorption in 800 nm, however, they are interesting as biomarker for protein and antibody.[18]

Among compounds mentioned before, porphyrins derivatives are the most used in PDT treatment due to their suitable photo-physical properties and due to their synthetic viability. Fig. 1 (a) displays a basic structure of the porphyrin. The structure of the porphyrin used in this work- (meso – Tetra(n-methyl – 4 –Pyridyl Porphine (TMTYP)) is depicted in Figure 2 (b). Generally, porphyrins display two absorption regions: Soret band, around 400 nm, and Q band in the range between 500-650 nm, as can be seen Fig.1b.

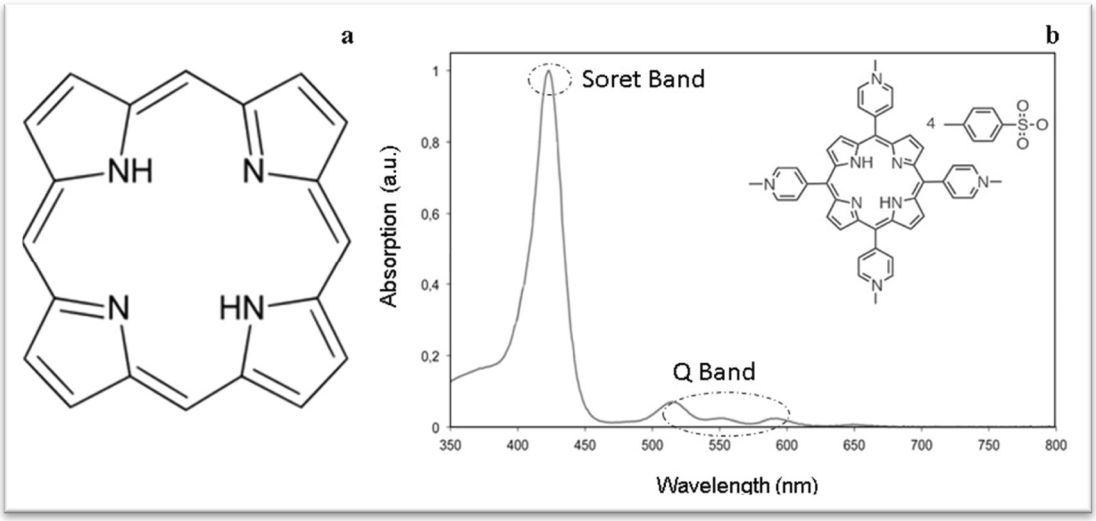

Figure 2 - (a) Basic structure of the Porphyrins - adapted from [23]. (b) structure and absorption spectrum TMTYP adapted from [24].

The porphyrins derivates have high affinity with lipoproteins of low density which are found in tumoral cells, i.e., they can preferentially accumulate in cancer cells.[23] Furthermore, the slightly acidic pH in cancer cells compared with health tissue is favorable once increase the porphyrins ionization that in turn become more soluble, and hence more selective for tumors.[24]

Although there are a lot of benefits in this treatment, and it is possible to synthesize good PS with both high absorption in the UV-vis region and high Singlet Oxygen yield, PDT treatment cannot be applied in deep tumors once most part of the PS absorbs the light in UV-vis range which, in turns,

has poor penetration in biological tissues (1-6 mm).[12] To overcome this issue, several solutions have been proposed in the literature as development of the Near-Infrared PS, micro-induced PDT, sonodynamic therapy (SDT), and X-PDT.[12]

The last therapeutic modality is the combination of RT with PDT in which a nanoscintilator is used to transform a high energy X-ray beam into visible light, the so-called scintillation or radioluminescence,[25] that can be absorbed by conventional PSs. As the focus of this work is development of nanodevices considering their scintillation properties with potential X-PDT application, a wider approach is necessary in follow sections.

2.2 Combined Radiotherapy and PDT (X-PDT): A new therapy modality

In a conventional RT cancer treatment, an electromagnetic radiation beam focuses the tissue region where is localized the tumor, with specific dose to cause cells damage and consequently leading cell death. First of all, the interaction between radiation and matter occur in a physics stage, that means ionization and excitation of the atoms. Then, in a physico-chemical stage the chemical bonds of the molecules are broken due to atomic ionization forming free molecules which can bind with others, this stage is called chemical stage. Lastly, in biological stage, biochemical and physiological changes are caused leading to morphological or functional organs changes.[26]

According to literature, cells death can happen by apoptosis, necrosis, or reproductive fail.[26]The necrosis occur when cells are seriously damaged (usually mitochondrias are the main affected), the cells swells and their membranes break. In the apoptosis process, the cell shrinks, and its nuclei is affected causing death. Lastly, in reproductive fail, due to ionizing radiation exposition, the cells cannot reproduce because of the damage, leading to death.[26] Once cell damage can affect both healthy and diseased tissues, RT procedure must be performed with the aim of killing tumor cells and preserve healthy tissues.

The mechanisms of cell damage by ionizing radiation can be direct or indirect.[26,27] The direct damage happens when ionizing radiation interacts directly with DNA molecules leading to the breakdown of the molecular structure, while indirect damage occurs when the ionizing radiation interacts with another molecules, specially water that is major compound present in the body.[26,27] In this case, free radicals are generated, and these species are extremely reactive due to unpaired electron in their structure.

In the X-PDT therapeutic modality a scintillator devices is used to transform a high energy beam in low energy photons, i.e., in UV- vis or infra-red range[25]. Thus, the compound must display fluorescence when interacting with X-ray and, hence activate the PS for ROS generation. Once PDT

treatment generate ROS by PS excitation, and considering that 33% of the DNA disrupting is due direct interaction with irradiation while others 67% are due free radicals – indirect damage,[26] the combination between RT and PDT can result in higher cell death than RT alone once X-PDT could enhance the ROS generation, increasing indirect damages.

Wang *et al* reported that X-PDT displayed greater performance to kill lung cancer cell than RT in *in vitro* and *in vivo* experiments. [15] Furthermore, other studies reported benefit effects in the use of scintillating nanoparticles to combine RT and PDT as high $^1O_2$ yield under x-ray irradiation (6MeV, 6Gy), ROS generation *in vivo* or *in vitro,* reduction of cancers cells viability among others[12,16,19,20,28]. Although results are promising, most (if not all) reported nanoscintillators still requires high doses of radiation to produce enough ROS. Therefore, research on developing more efficient nanoscintillators is still a quite active area due to the potential ability to improve cancer treatment and for this end fluorescence and radioluminescence mechanism's knowledge are required.

2.3 Fluorescence and X-ray Excited Optical Luminescence - XEOL

Luminescent materials have been widely used in biochemical and biophysics field, as for instance, obtaining medical images, diagnostics, DNA sequencing, forensics, among others and thus, fluorescence spectroscopy has been development during last decades.[29,30] According to literature, fluorescence is one of the luminescence categories that is the emission of light by a material in excited state. The Fig.3a display a absorption and luminescence spectra of the anthracene - that was chosen as fluorophore in this work – and as it can be seen, the light emission can occur by fluorescence or phosphorescence.[30,31] The difference between them is the kind of the transition as illustrated by the Jablonski diagram (Fig. 3b). In this diagram it is possible to see singlet ground state (S_0) and excited singlet state (S_1) - characterized by electron paired in opposite spin orientation – and triplet state (T_1) that is characterized by electrons with the same spin orientation. The changing of the spin orientation is called intersystem crossing. If the electronic transition is from a singlet excited state (S_1, S_2) to a singlet ground state (S_0) followed by photon emission we have a fluorescence phenomenon whereas if the electronic transition happens from triplet excited state (T_1) to singlet ground state (S_0) we have phosphorescence. Although both occur with photon emission, the emission rate of fluorescence (10^8 s^{-1}) is higher than the emission rate of phosphorescence (10^3 to 10^0 s^{-1}).[30,32]

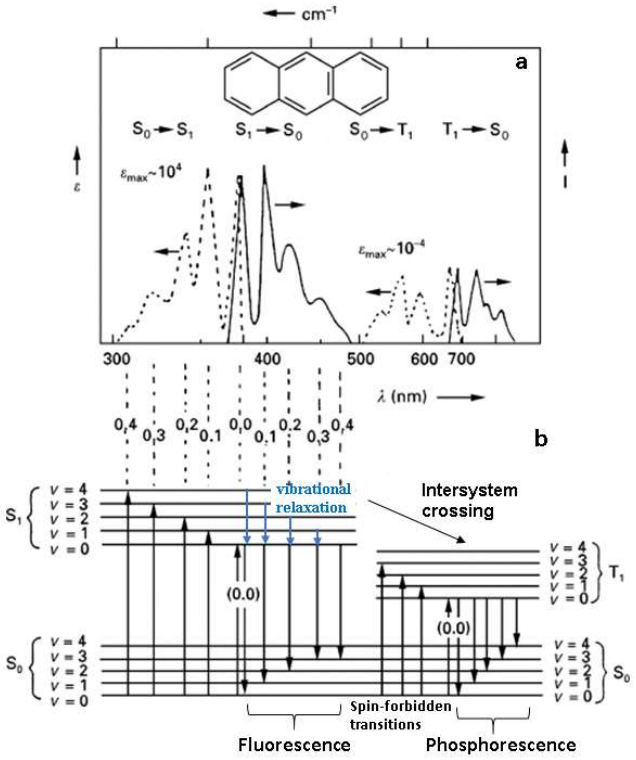

Figure 3 - Anthracene absorption (dashed lines) and emission (solid lines) spectra, and b Jablonski diagram modified for anthracene. Adapted from [31]

The Singlet and Triplet states are named in this way due to the multiplicity (M) spin rule. According to this rule, the multiplicity depends on the total spin quantum number and can be calculated by the following equation:

$$M = 2 \times S + 1$$

where $S = \sum s_i$, and s_i is spin number (+1/2, -1/2). Then, considering two electrons with opposite spin (+1/2, -1/2) in a ground state, and one of them undergoing a transition to an excited state without spin change. For both excited and ground state, the spin multiplicity is one, S = 0 and M = 1, these are Singlet states and this kind of the transition is called Singlet-Singlet transition. When one of these two electrons changes its spin direction when undergoing transition to an excited state (+1/2, +1/2), we have a singlet in ground state (S = 0 and M =1) whereas the excited state is a triplet state once S = 1 and M =3 that means spin multiplicity of three, in this case. The electron spin transition with change in spin direction is named Singlet-Triplet transition.[29]

Furthermore, each electronic state may have sublevels of energy (1, 2, 3) related to the vibrational states. In addition, Singlet-Singlet and Triplet-Single transitions between vibrational levels – vibrational relaxation - can also happen. In this sense, when an electron absorbs energy and is

promoted to any vibrational energy level in the excited state, it returns to lowest vibrational level. Then, from this level, it can return to the ground state with photon emission.[29]

According to the Franck-Condon principle, electronic transitions are more likely to happen without any changing of the molecule nuclei position in the ground state and, as consequence, the probability of the specific transition in absorption will be the same for emission[29]. As a consequence, the electron returns to the same vibrational level in ground state and hence the emission is a mirror of the absorption. The mirror image can be seen in the absorption and fluorescence spectra of several luminescence material, as for instance, anthracene.

Fig. 3a displays the mirror rule applied to anthracene. The dash lines are related to the absorption transitions while solid lines are related to emission in the spectra. In the first absorption transition (0,4), electron undergo to excited state crossing three vibrational level until reaches fourth, thus when the electron comeback to ground state must across necessarily three vibrational levels too until reach next vibrational level. Therefore, the number of the vibrational levels that the electrons cross during the absorption must be the same when these electrons return to ground state leading a mirror image between absorption and fluorescence spectra.[29]

However, not all emitted light is classified as fluorescence because according to literature, for Singlet-Singlet transition the extinction coefficient is 8-fold higher compared to Triplet-Singlet transitions, indicating that Singlet-Singlet is associated to spin-allowed transition and, thus, for anthracene, the emission in the first region - λ <500 nm – are due fluorescence. The lower extinction coefficient in the region λ > 500 nm is associated to spin-forbidden transitions, resulting in light emission by phosphorescence.[32] Therefore, anthracene emission spectrum is composed by fluorescence and phosphorescence emissions.

In addition, for anthracene, light emission can also occur due to the interaction with X-ray (scintillation). Fig. 4a shows a schematic illustration of the interaction between X-ray and materials. When an X-ray beam reaches an atom, the radiation can be absorbed followed by re-emission in different direction of the incident beam in an elastic process named Rayleigh scattering. No energy is absorbed in a Rayleigh Scattering. Energy from the incident X-ray beam can be absorbed by the photoelectric effect, Compton scattering, and pair-production, depending on the energy of the X-ray photons and the atomic number of the material. In photoelectric and Compton effects, electrons absorb energy from the X-ray photons and are ejected from the atom, delivering their kinetic energy to the medium along their tracks.

When electrons are ejected from a given atom in a photoelectric or Compton process, holes are created in an atomic orbital and hence an electron from higher level can fill the hole leading to X-ray fluorescence (characteristic X-ray), or, instead of the atom emitting characteristic X-rays, if the photon

is absorbed by another electron, Auger electron is ejected from the atom. It is important to emphasize that the effects due interaction between electromagnetic wave with the matter depends on the energy of the beam. Lastly, another effect happens when outer electron scatter X-ray with partial energy transfer to the recoiling electron, known as Compton scattering (elastic).[28]

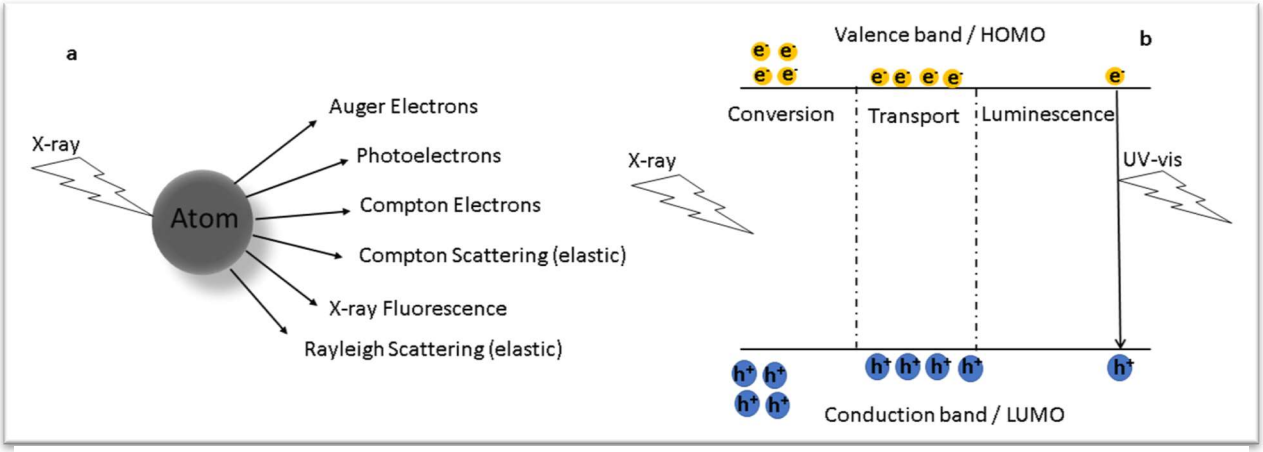

Figure 4 - a, Effects of the interaction between x-ray and materials and b, XEOL steps in a scintillator: conversion, transport, and luminescence

Once main effect studied in this work is X-ray Excited Optical Luminescence (XEOL), deeper approach for this phenomenon is suitable to know the mechanism of the light emission due interact between X-ray and a scintillator. In this sense, as can be seen in Fig. 4b, scintillation emission by a semiconductor occurs in three consecutives steps: conversion, transport and luminescence.[25] Firstly, in the conversion step, under X-ray irradiation a big amount of the free electron and holes are generated specially in the inner shells due primordially photoelectric effect and Compton scattering. Then, in a transport stage there are diffusion of the electron-hole pairs through the semiconductor. Gradually, the electrons move to conduction band or LUMO - in case of the molecules - band while the holes migrate through the valence band or HOMO -in case of the molecules - band. Finally, radiative recombination between electrons and holes generates X-ray luminescence. Non-radiative transitions can also take place, depending on the scintillator quantum yield (QY).[28,33]

In this sense, for therapeutic applications of nano scintillators high QYs is necessary, because higher light emission leads more ROS generation that in turn improves the cancer death efficacy. Besides high quantum yield, high atomic number (Z) is also desired for scintillators to enhance conversion of high energy beams into UV-vis photons, due to the larger X-ray attenuation and absorption coefficients of high Z materials. Thus, a good scintillator is that one which have great interaction with X-ray leading a high light emission. Furthermore, for better performance in X-PDT, it is important to have a good overlap between fluorescence of the scintillator and absorption spectrum of the photosensitizer, to ensure activation of the PS and hence ROS generation.[28,12,20]

However, compounds that simultaneously combines high Z and high QY are rare. Although Sodium Iodide present these two properties, it is highly hygroscopic, hindering the production of NaI nanoparticles and their use in aqueous biological mediums.[8,34] To compensate the low atomic number of organic scintillators and still take advantage of their high QY, they can be loaded with high Z atoms[35] by simple mixture or more sophisticated protocols to produce hybrid-nanoparticles.

Thus, the presence of the metallic nuclei in hybrid structures increases Z, improving the interaction with X-ray, besides enhancing fluorophore luminescence by plasmonic effect. Moreover, considering the possibility to maximize light emission by the presence of metal nanoparticles in a semiconductor hybrid system, it is necessary to introduce the mechanisms of plasmon-enhanced luminescence.

2.3.1 Fluorescence and XEOL enhancements in Hybrid materials

The luminescence enhancement observed when a luminescent center is placed near a noble metal nanostructure is associated to a plasmonic effect which happens due to the collective oscillation of the free electron cloud of the metallic nanoparticles in resonant conditions. According to literature, there are two mechanism for luminescence enhancement.[36,37] The first one occurs due to the strong interactions between free electrons of metal nanoparticles and light waves. Once the size of the metallic nanoparticle is smaller than the wavelength of the incident light, when light propagates through the metal particle, the free electrons collectively oscillate according to the light electric field, known as Localized Surface Plasmon Resonance (LSPR) (Fig. 5a), leading to a plasmon band that can be detected by UV-vis spectroscopy[38,39] The light absorption and/or scattering is associated with LSPR and affect the luminophore near to the metallic nanoparticles leading to a Metal Enhanced Fluorescence (MEF).[40,1,41, 42]

The plasmon resonance increases the density of the local electric field compared with non-resonant conditions – Fig. 5 b, c ; which increases the fluorophore excitation near to the metal nanoparticles – Fig. 5 c - and hence enhance its light emission.[41,42] This mechanism require partial or total overlap between fluorophore excitation spectra and metallic plasmonic band.[38]

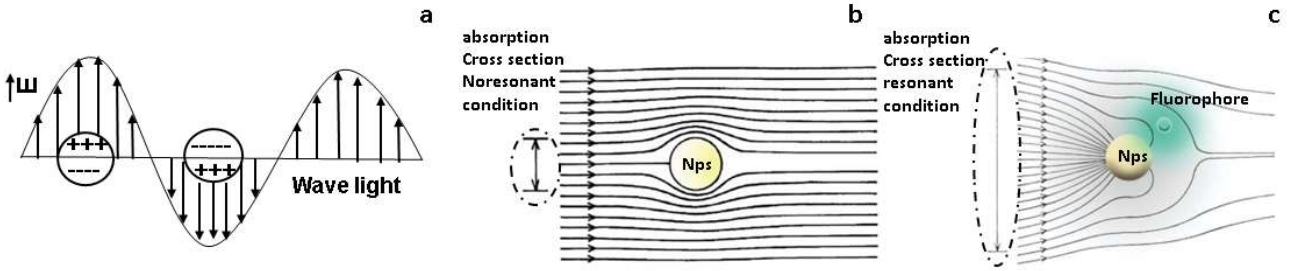

Figure 5 - plasmonic oscillation of the free electron cloud in surface of metallic Nanoparticles (Nps) due to electric field of the incident light propagating through the Nps; b, energy flow around of the Nps in non-resonant condition, b and in resonant condition, c. Is possible to see larger absorption cross section – vertical lines – for resonant condition and a fluorophore near to Nps. Adapted from [36, 37]

The second mechanism is characterized by an energy transfer from the luminophore in excited state to the plasmon in the metal nanoparticles,[41] that in turn irradiate the energy to the far field. Similar to the phenomenon known as Foster Resonance Energy Transfer in which energy is transferred from a donor in excited state to an acceptor in ground state[30]. In this case, it is necessary an overlapping of the donor fluorescence emission with acceptor absorption spectra.[30,39,42]

Besides enhancing fluorescence by the MEF effect, hybrid metallic-organic structures can display higher interaction with X-ray due to the higher Z of the metal nanoparticles which can increase the radiation dose absorbed by the scintillator material and/or to by targeted cells. Therefore, hybrid-structures of the anthracene and metal nanoparticles could present potential applicability in X-PDT.

2.3.2 Dose Enhancement Factor in Hybrid materials

Considering a monoenergetic beam of electromagnetic wave with initial intensity I_0 and intensity I (after interacting with the material), crossing any material of the thickness x, the attenuation obeys the following exponential law:

$$I = I_0 \times e^{-\mu x}$$

where μ is linear coefficient attenuation and depend on the material density (ρ), i.e, the value change according to physical state of the compound. Because of this, it is interesting use mass attenuation coefficient (μ/ρ).[26] In this sense, heavy materials can interact more with ionizing radiation because of their higher atomic number, improving the effects due interaction between radiation and materials. In photoelectric effect, for instance, when ionizing radiation reach an atom, its absorbed and an electron is ejected from its inner shell, the energy is deposited in the environment that leading to the absorbed

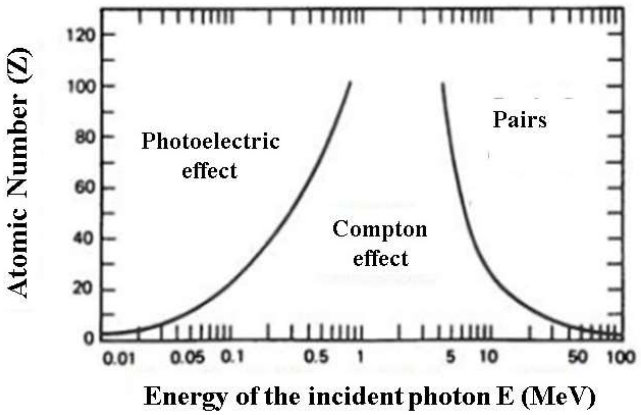

Figure 6 - Main ionizing radiation effects as function of the attenuator atomic number and energy beam. Adapted from [28]

dose.[43] Since radiation absorption depends on the mass attenuation coefficient (μ/ρ), materials with high atomic number can absorb more ionizing radiation.[44] Fig. 6 depicts the relationship between energy range and atomic number, that means, atoms with higher Z, interact with X-ray predominantly by photoelectric effect since the energy range of the X-ray is lower. Considering, for instance, gold (Z=79) the photoelectric effect is predominant in a large X-ray energy range that in turn can lead higher dose enhancement in the environment.

In this sense, metal nanostructures have been employed to enhance the delivered radiation dose.[45,46] Gold nanoparticles, for instance, demonstrated to be able to improve radiotherapy in *in vivo* experiment.[47] In order to detect and the quantify dose delivered, radiation sensors have been employed and Electronic Spin Resonance (ESR) measurements have been performed.[48,49] In this case, a compound generate a free stable radical under ionizing irradiation that in turn are detected by ESR, displaying a specific signal.

Then, comparing the ESR intensity of pure sensor with the ESR intensity of sensor containing materials with high Z, is a powerful method to infer about the dose enhancement factor (DEF) prompted by the nanoparticles[50,51]. The DEF can be calculated by considering the quotient between the peak-to-peak amplitude of the central line of the ESR spectra of the samples with and without hybrid nanoparticles.[50]

2.4 Anthracene and Hybrid Anthracene nanoparticles

Organic fluorescence materials have been widely used as probe in chemical, biological, physic-chemical environment, specially anthracene and its derivatives once this compound presents high fluorescence and scintillation yield.[52,53] Anthracene is a Polycyclic Aromatic Hydrocarbon (PAH), which consists a class of organic compounds with two or more fused aromatic rings and/or pentacyclic

rings arranged in linear, angular, or cluster formation[54] and is commonly used as reference material to determine relative scintillation efficiencies of others scintillators.[34]

The PAHs are a result of human activity as wood, oil, coal, and organic matter combustion and natural process as Vulcanic eruption carbonization. There are more than 100 PAHs known recently, 16 of them receive more attention due to their high incidence and / or toxicity and anthracene is among those most incident[54]. Despite anthracene being part of the PAH group known as carcinogenic, toxic and contaminant; according to United States Environmental Protection Agency (USEPA), anthracene is classified in the group 3 as non-classifiable as carcinogenic to humans.[54] Furthermore, experiments *in vivo* have shown that anthracene was not lethal even under high concentrations [55].

Although many types of nanoscintillators have been developed[56], like lanthanide-based nanoparticles and quantum dots[28], nanoparticles of traditional organic scintillators, like anthracene and their derivatives, have never been produced and investigated for X-PDT applications, revealing that research in this field is still required. Furthermore, the blue emission of anthracene coincides with the absorption of most porphyrins – used as PS - once the Soret band, present in all of the porphyrins (350 – 450nm), is due electronic transition of their basic structures.[57] Therefore, considering these relevant properties of anthracene, its applicability in X-PDT should be verified.

Besides be noteworthy as great scintillator, anthracene can act as a photosensitizer leading to ROS generation under UV-vis irradiation that in turn causes intracellular oxidative stress, mutation, cell death.[58,54,55] This behavior is expected for a good PS in PDT and thus, these features make more relevant the researches aiming to use it in X-PDT treatment. A metal core in these structures could absorb the X-rays, transferring energy to the organic compounds that, in turns, produce Reactive Oxygen Species (ROS). In this sense, combining the X- ray luminescence from anthracene with metal nanoparticles can be useful for biomedical application.[35,59] However, the use of the anthracene and their derivates as nanoparticles has not been reported. It should be emphasized that, besides being considered a good scintillator, anthracene can also act as carrier of the $^1O_2$[60], evidencing that such hybrid nanostructures could have multiple functions when it comes to combine radiation and photodynamic therapies.

The development of the anthracene nanoparticles could improve their selectivity for cancer cells due the Enhanced Permeability Effect, caused by the hypervascularization of cancer tissues that allows accumulation of particles in the nanoscale. Furthermore, because anthracene is insoluble in water, anthracene nanoparticles consist a colloidal dispersion that allows surface modification and functionalization, which is essential for biomedical applications.

In summary, to enhance the luminescence properties of the anthracene nanoparticles since their interaction with X-rays is low, hybrid-systems consisting of a metal core and a layer of anthracene (shell), are promising nanodevices to achieve increased interaction with ionizing radiation, increased

fluorescence and scintillation intensities and hence higher yield of $^1O_2$ generation when combined with porphyrins - scheme 1. In this context, core-shell nanoparticles consisting of noble metal core and an anthracene shell could be employed to increase the interaction of X-rays with the organic scintillator due to the high Z core, leading to the so called dose-enhancement factor (DEF).[61] Once scintillation intensity depends on the dose-rate of the X-ray beam, the DEF could increase scintillation intensity by increasing the dose rate at the anthracene layer.

Besides increasing the atomic number, the noble metal core could increase luminescence emission from the anthracene layer by plasmon-enhanced luminescence.[62,38] The collective oscillation of the free-electron cloud at the nanoparticle surface upon incidence of light in resonant conditions increases the local electric field, leading to Metal Enhanced Fluorescence (MEF).[40,1,41, 42] Together, DEF and MEF could synergistically increase scintillation emission and $^1O_2$ production – scheme 1b allowing for the combination of RT and PDT in a single nanodevice. If the anthracene layer is thin enough, the electron ejected by the metal core can also increase the dose in the tumor volume, leading to increased radio sensitization by the local dose enhancement and *in-situ* $^1O_2$ generation.

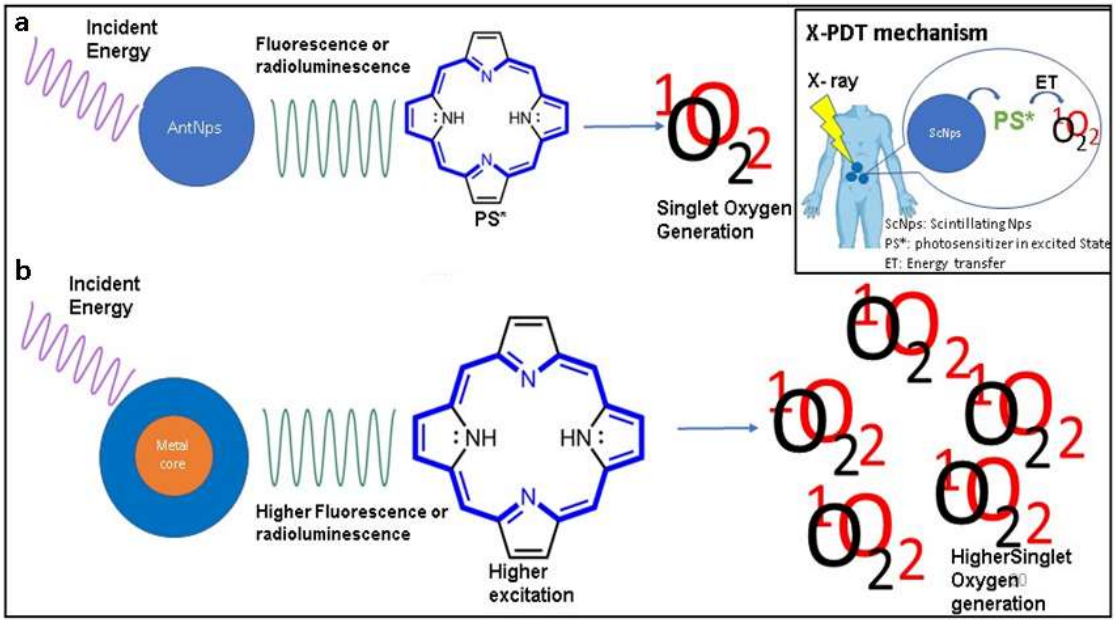

Scheme 1 – Interaction of the anthracene, a and metal@anthracene, b light emission with porphyrin (PS*) leading to singlet oxygen generation by an energy transfer from the excited state porphyrin to molecular oxygen . The presence of the metal in the hybrid structures, b could increase singlet oxygen generation due both MEF and DEF effects.

2.5 Objective

In this work, anthracene and hybrid Ag/Ant and Au/Ant nanoparticles are synthesized and characterized to verify their potential applications as a nanoplatform to combine RT and PDT

treatments. Fluorescence properties of these nanoparticles were explored and the metal enhanced fluorescence of the hybrid systems as well as their ability to generate and trap $^1O_2$ were investigated. The $^1O_2$ production and its interaction with anthracene and Ag/Ant under UV-vis and X-ray irradiation were investigated by Electron Spin Resonance (ESR) technic to evaluate the potential applicability in X-PDT cancer treatment. In this sense it was expected:

- Fluorescence enhancement for metal@anthracene due plasmonic effect.
- AntNps fluorescence able to induce singlet oxygen generation in presence of porphyrin;
- Higher singlet oxygen generation for metal@anthracene;
- Higher interaction with X-ray for metal@anthracene due to DEF effect;
- Evaluation of using the nanoparticles for multitherapeutic approaches;

3. Materials and methods

Anthracene and chloroauric acid ($HAuCl_4$) were purchased from Sigma-Aldrich. Sodium borohydride ($NaBH_4$) and silver nitrate ($AgNO_3$) were provided by Vetec (Brazil) and Cennabras, respectively. meso-Tetra(*n*-methyl-4-Pyridyl) Porphine (TMTYP) was acquired from Midcentury Chemicals. 2,2,5,5-Tetramethyl-3-pyrroline-3-carboxamide (TPC) was supplied by Sigma-Aldrich. DL-alanine (99%) was obtained from Acros Organics

3.1 Preparation of anthracene nanoparticles.

Anthracene nanoparticles (AntNps) were synthesized by a sonochemical method[63]. To this end, 1 mL of 4 mmol L^{-1} anthracene solution in ethanol was added to 10 mL of Milli-Q^{TM} water under sonication for 30 min at room temperature, 25°C. The colloidal dispersion was whitish and turbid, which is characteristic of nanoparticle dispersion[63]. The dispersion was kept overnight for the colloidal solution to stabilize.

3.2 Synthesis of silver and gold nanoparticles.

Stock solutions of silver and gold nanoparticles (AgNps and AuNps, respectively) were prepared by chemical reduction. To synthesize AgNps, 200 mL of 2 mmol L^{-1} $AgNO_3$ and 1.25 g L^{-1} poly(vinyl alcohol) (PVA) solution was added to 200 mL of 4 mmol L^{-1} $NaBH_4$ solution under vigorous stirring at room temperature (25°C), to yield a yellow colloidal suspension characteristic of AgNp dispersion[64]. The PVA act as stabilizing agent leading to steric stabilization. To synthesize AuNps, 200 mL of 2 mmol L^{-1} $HAuCl_4$ solution was added to 200 mL of 4 mmol L^{-1} $NaBH_4$ solution under vigorous stirring at room temperature – 25°C[50]. The color of the solution changed to red, indicating that colloidal Au was formed. Both the AgNp and AuNp solutions were kept under stirring for 12 h. To eliminate reactional

residues, 200 mL of AgNp or AuNp dispersion was dialyzed in 5 L of Milli-Q^{TM} water for five days; water was replaced daily. Plasmon absorption peaks for Ag (400 nm) and Au (530 nm) were recorded in an Ultrospec 2100 pro (Amersham Pharmacia), confirming that the syntheses were successful.

3.3 Synthesis of hybrid Ag@anthracene and Au@anthracene nanoparticles.

Hybrid Ag@anthracene and Au@anthracene nanoparticles, designated Ag@AntNPs and Au@AntNps, respectively, were synthesized by mixing Milli-Q^{TM} water and AgNp or AuNp stock solution. For Ag@AntNPs, 0.5, 0.8, 1, 2, 4, or 10 mL of AgNp solution was completed to 10 mL with Milli-Q^{TM} water, to give AgNp concentration of 0, 0.05, 0.08, 0.1, 0.2, 0.4, or 1 mmol L^{-1}, respectively. For Au@AntNPs, 0.5, 1, 2, 4, or 10 mL of AuNp solution was completed to 10 mL with Milli-Q^{TM} water, to give AuNp concentration of 0, 0.05, 0.1, 0.2, 0.4, or 1 mmol L^{-1}, respectively. Then, under sonication, 1 mL of anthracene solution was added to each sample, and sonication was maintained for 30 min. Before the experiments were carried out, all the samples were kept in an open vial overnight at room temperature – 25°C.

3.4 Characterization of samples.

Dynamic light scattering (DLS) was conducted on a Zeta-Sizer system (Malvern Instruments). A fixed wavelength (633 nm, He–Ne laser) and angle (90°) were employed to record the particle size distribution and the average particle size of all the samples. Atomic Force Microscopy (AFM) images were collected with the Shimadzu model SPM-9600 scanning microscope (Scanning Probe Microscope) operating in phase; i.e, intermittent contact, at room temperature and in air. The samples were dripped onto freshly cleaved mica substrate. Fluorescence spectroscopy was performed with a Hitachi F-7000 spectrofluorometer equipped with a 150-W xenon arc lamp and 700-V photomultiplier tube; a quartz cuvette was used. The as-prepared samples were diluted 100 times to avoid inner-filter effects. The excitation and emission monochromator slits were 10 nm.

3.5 Singlet Oxygen generation and trapping under UV-vis light and X-rays

Singlet Oxygen ($^1O_2$) generation induced by nanoparticle fluorescence was verified by using TMTYP, whose Soret band matches the maximum emission wavelength of anthracene. To detect $^1O_2$, Electronic Spin Resonance (ESR) was accomplished by using 2,2,5,5-tetramethyl-3-pyrroline-3-carboxamide (TPC) as spin-trap; a methodology described in the literature was followed[65]. According to this methodology, TPC can react with singlet oxygen leading a characteristic ESR signal with intensity proportional to the amount of the $^1O_2$ generated. Therefore, considering our hypothesis

anthracene and metal@anthracene nanoparticle could excite the TMTYP molecules inducing singlet oxygen generation which is then trapped by TPC. It is worth mentioning that this spin-trap was chosen because of its high specificity for singlet oxygen even in lower concentration. Thus, 1 mol L^{-1} TPC stock solution was prepared by diluting 168 mg of TPC in 1 mL of Milli-Q^{TM} water and kept in a freezer to avoid oxidation. The ESR properties of the irradiated samples were measured on a JEOL-JES-FA 200 (9.5 GHz) spectrometer. The measurement parameters were as follows: room temperature, central field at 338.5 mT, microwave power = 5mW, sweep time = 1 min, sweep width = 10 mT, modulation amplitude = 0.1 mT, magnification = 1000×, and time constant = 0.3 s. Three scans were taken for each sample.

To verify energy transfer from the AntNps to the porphyrin, 85.5 µL of 1 µM TMTYP solution was mixed with 35.5 µL of 0.4 mM nanoparticle dispersion (AntNps or 0.08 mol L^{-1} AntNps) and 12 µL of TPC stock solution and irradiated with an XBO 75W/2 Ofr, Osram Xe lamp and a filter band pass (transmission between 200 and 385 nm), to excite anthracene but not the porphyrin. The samples were irradiated for 60 min, and the ESR spectra were recorded at 5, 10, 30, and 60 min of irradiation to detect $^1O_2$ generated in the AntNp-TMTYP system. To ensure that $^1O_2$ generation was not due to direct porphyrin excitation, a control experiment was performed by using 85.5 µL of 1 µM TMTYP solution mixed with 35.5 µL of Milli-Q^{TM} water and 12 µL of TPC stock solution, in the absence of AntNps.

To investigate $^1O_2$ trapping by AntNps, $^1O_2$ was generated by direct excitation of TMTYP. To this end, 85.5 µL of 1 µM TMTYP solution was mixed with 35.5 µL of AntNp dispersion (AntNps or 0.08 mol L^{-1} AntNps) and irradiated with the same Xe lamp, but a different band pass filter (transmission between 400 and 500 nm was used). Reaction of $^1O_2$ with anthracene forms an endoperoxide, suppressing anthracene fluorescence.[66] The fluorescence spectra were measured at 375-nm excitation, at 5, 10, 30, and 60 min of light irradiation.

To verify $^1O_2$ generation under irradiation with X-rays, AntNps or 0.08 mol L^{-1}Ag@AntNps were centrifuged and resuspended in 100 µL of Milli-Q^{TM} water. Then, 35.5 µL of the concentrated AntNp dispersion was mixed with 85.5 µL of 3.3 mM TMTYP solution and 12 µL of TPC stock solution. Two control samples were also prepared: one containing 85.5 µL of 3.3 mM TMTYP solution, 12 µL of TPC stock solution, and 35.5 µL of Milli-Q^{TM} water; and one containing 12 µL of TPC stock solution and 121 µL of Milli-Q^{TM} water. The samples were irradiated by using an X-Ray tube (Magnum-Moxtek, USA) operating at 48 kVp and 0.2 mA; cumulative doses of 30, 60, 90, or 120 Gy were used.

3.6 Dose enhancement experiments under X-rays

Dose enhancement caused by the metal nanoparticles was investigated by Alanine/ESR dosimetry.[51] Considering higher Z of the Au compared to Ag, gold nanoparticles are better to optimize x-ray interaction, leading to higher local dose enhancement. For this reason, AuNps were chosen to perform DEF experiments. To this end, 400 mg of alanine was added to 20 mL of 1 mol L^{-1} Au@AntNps, stirred for 10 min, and dried at 40 °C for 24 h, to produce alanine samples with 1% Au (in mass). For the control sample, 400 mg of alanine was diluted in 20 mL of Milli-Q™ water and dried at 40 °C for 24 h. Then, the powders were encapsulated and irradiated with an X-ray tube (GE-Isovolt Titan E-160M-2) operating at 80 kVp (effective energy of 31 keV). The X-ray dose rate at the sample position was around 0.55 Gy/min. Cumulative doses of 10, 20, 30, 40, 50, or 60 Gy were employed.

The ESR spectra were acquired on a JEOL JES-FA 200 (9.5 GHz) spectrometer, in triplicate. Approximately 35 mg of the sample was placed in a quartz tube and positioned in the center of the standard JEOL cylindrical cavity to guarantee that the whole sample was inside the active volume of the ESR cavity. The ESR parameters employed for the measurements were fixed, as follows: room temperature, central field = 338.5 mT, microwave power = 5 mW, sweep time = 1 min, sweep width = 10 mT, modulation amplitude = 0.4 mT, magnification = 100×, and time constant = 0.3 s. Three scans were taken for each sample. To compare the signal amplitudes of the different samples, the spectrum of each nanocomposite was normalized by the total mass of the respective sample. The ESR intensity was adopted as the peak-to-peak amplitude of the mass-normalized ESR spectrum of alanine. The Experimental Dose Enhancement Factor (DEF) was calculated as the ratio of the slopes of the dose-response curves of the sample with and without Au@AntNps.[50]

4. Results and Discussion

We synthesized anthracene nanoparticles (AntNps) by a sonochemical method that employs ultrasound waves to generate acoustic cavitation for nanoparticles to nucleate and to grow. We used this method because addition of anthracene diluted in ethanol to water under sonication changes the medium polarity, so that nucleation accelerates and growth slows down, producing AntNps.[63] The resulting colloidal dispersion was whitish and turbid because AntNps scattered light.[63] In addition, when sound waves propagate in a liquid, they cause dynamic stress, leading to acoustic cavitation. The size of the bubbles formed in the solvent increases to a certain limit, and the bubbles later collapse during contraction. When bubbles arise, grow, and collapse, extreme conditions such as high temperature, pressure, and shock waves emerge, giving rise to small nuclei and thus preventing aggregation[63,67]. Compared to the conventional stirring method, sonication accelerates nucleation, decreasing the average

nanoparticle size[63]. According to the literature, sonication produces smaller, and more monodisperse particles than conventional magnetic stirring.[63]

We characterized AntNps, Ag@AntNps, and Au@AntNps by DLS measurements (Figures 7a and b) and AFM images (Figures 8a, b, c, and d). On the basis of Figures 7a and b, AntNPs presented broad particle size distribution, from 220 up to 820 nm, with average particle size of 370 nm, whereas AgNps and AuNps had average particle size of 14.5 and 17 nm, respectively. For Ag@AntNps and Au@AntNps, the average particle size decreased upon increasing amount of AgNps or AuNps respectively (Figures 7a and b). In other words, DLS revealed that addition of AgNps or AuNps reduced the hydrodynamic radius of the Ag/anthracene or Au/anthracene colloidal dispersion, suggesting that AgNp or AuNp acted as a seed around which the anthracene layer grew, to culminate in a core-shell structure.

A similar behavior has been observed for Au@ZnO and Ag@ZnO nanocomposites and for Ag, Au, or Pt covered with a polymer shell in hydrophobic and hydrophilic hybrid structures[68,69]. Guidelli et al. showed that, in the presence of metallic nanoparticles (AgNps or AuNps), ZnO nucleates on the metal nanoparticles suspended in solution. SEM back-scatter images confirmed this nucleation and revealed that the metal nanostructure is located in the center of the ZnO particles, leading to a core-shell structure. Fratoddi et al. also showed that several polymer shells grow in hydrophilic and hydrophobic hybrid systems bearing Ag, Au, or Pt as core, demonstrating that the polymers and the metal nanoparticles interact[69]. Moreover, a recent work reported that a silica (SiO_2) shell emerges around AuNps after hydrolyses and polymerization. Up to a given concentration, increasing amount of Au core preferentially yields single-core particles; thereafter, multi-core particles arise. Increasing amount of Au core also affords thinner silica shells; i.e, the hybrid particles become smaller.[70] Our hybrid Ag@AntNps and Au@AntNps behaved similarly, as pointed out by the DLS results.

Higher nucleation rates reduce nanoparticle size, so a higher amount of nuclei in the beginning of the synthesis should lead to smaller particles in the colloidal dispersion[63,67,71,70]. Higher amount of AgNps or AuNps in Ag@AntNps and Au@AntNps, respectively, should provide smaller hybrid particles if AgNps or AuNps acted as nucleation sites. DLS measurements gave the following average particle size for Ag@AntNps: 370, 356, 164, 130, 99, 85, and 57 nm for 0, 0.05, 0.08, 0.1, 0.2, 0.4, and 1 mmol L^{-1} AgNps, respectively (Figure 7c). Concerning Au@AntNps, the average particle size was 347, 335, 255, 174, 126, and 76 nm for 0, 0.05, 0.1, 0.2, 0.4, and 1 mmol L^{-1} AuNps, respectively (Figure 7d). These results evidenced that particle size in the colloidal dispersion decreased upon rising AgNp or AuNp concentration because the concentration of nuclei for AntNp growth went up.

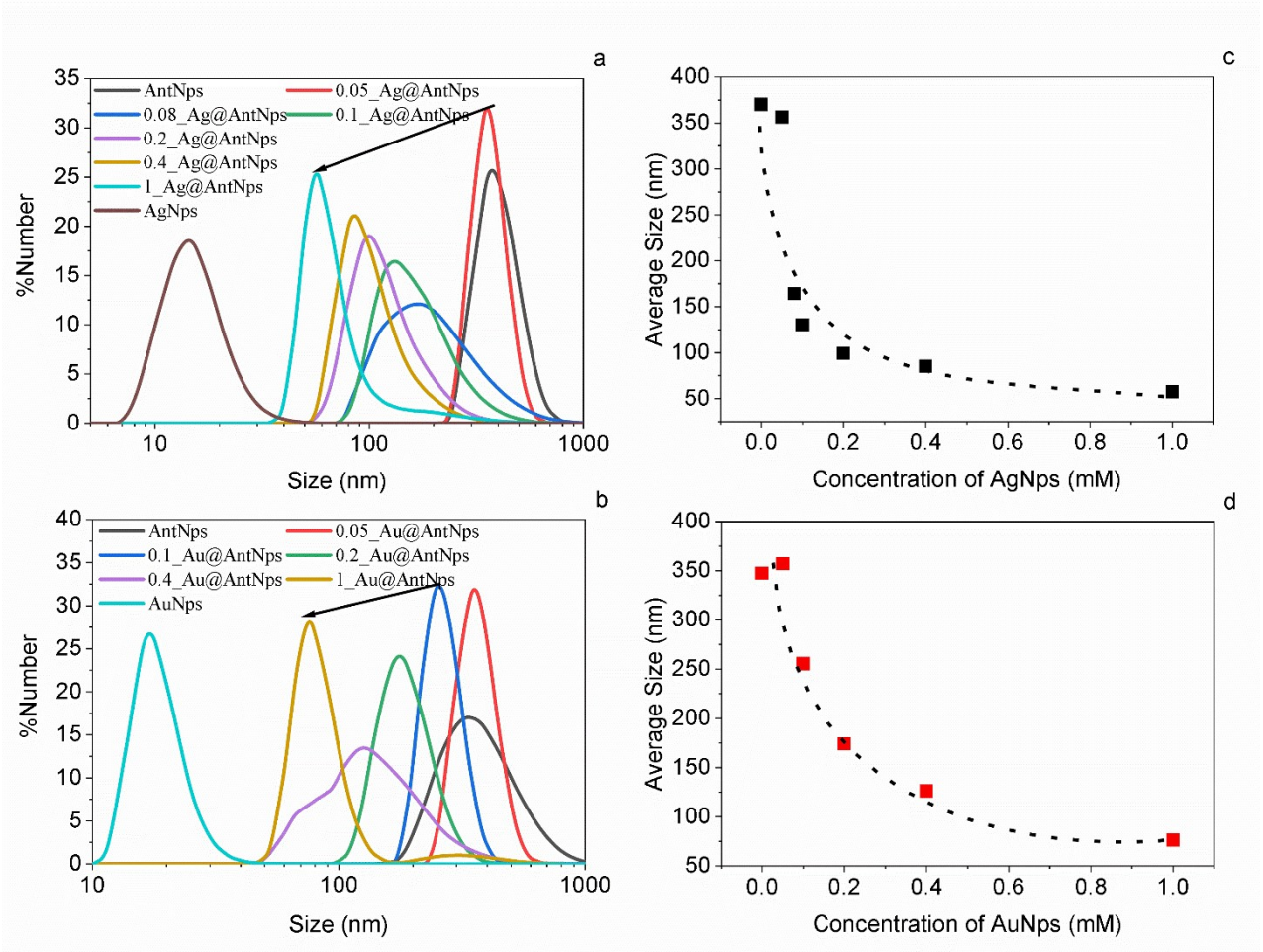

Figure 7 - Particle size distribution of the nanoparticles produced with varying concentrations of silver (a) and gold (b) nanoparticles. The total volume was fixed at 10 mL. Average sizes of the hybrid nanoparticles containing silver (c) and gold (d) for differ ent AgNp and AuNp concentrations in mmol L^{-1}

To confirm this hypothesis, we acquired AFM images for AntNps, Ag@AntNps, and Au@AntNps. On the basis of Figure 8a, AntNps consisted of polymer aggregates with non-defined morphology. To observe how AgNp and AuNp influenced AntNp growth, we decided to use 1 mmol L^{-1} AgNps or 1 mmol L^{-1} AuNps because this concentration provided smaller average size of nanoparticles, as evidenced by the DLS measurements. By applying the phase contrast mode, we obtained images that revealed regions with different viscoelastic properties, attributed to differences in composition. The lightest points corresponded to the regions of the sample with the largest viscoelasticity, while the darker points referred to the regions with the lowest viscoelasticity. Given that viscoelasticity is associated with differences in the composition of the sample, the solid/hard metal nanoparticles appeared as darker points in the images (lower viscoelasticity) and were surrounded by a clearer light-yellow layer, which corresponded to the polymer layer of anthracene (larger viscoelasticity), indicating that core-shell structures were formed.

Figures 8b and c show the presence of some uncovered AgNps (dark/black spots/particles), whereas Figure 8d evidences the presence of multi-core Au@AntNps. A possible explanation is that, as mentioned above, the samples imaged here were the ones with the highest AgNp or AuNp content. Other authors[70,72] described that high concentrations of metal nanoparticle core produce multi-core hybrid nanoparticles. Given that the concentration of anthracene was the same for all the samples synthesized here, the presence of uncovered AgNps could have resulted from the high concentration of colloidal metal, too.

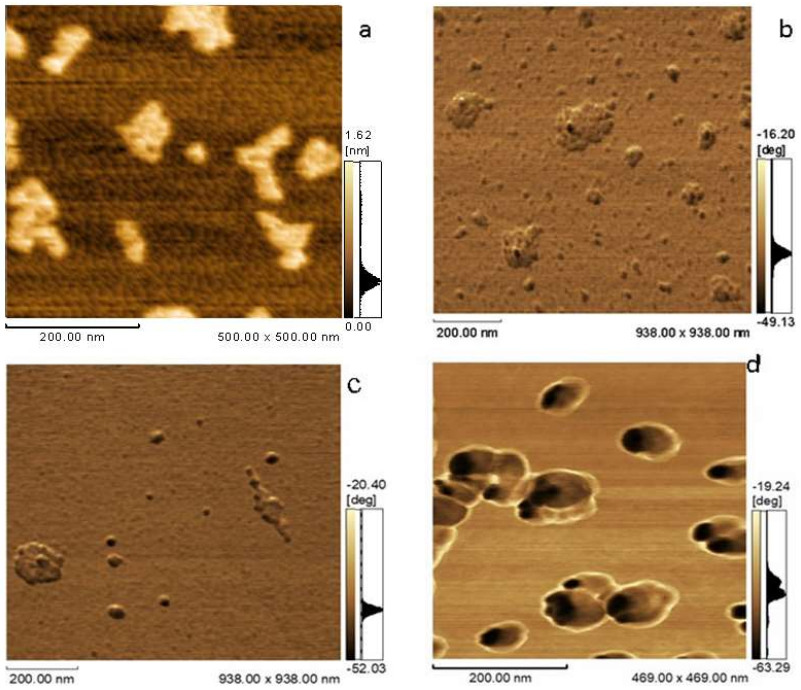

Figure 8 - AFM images of AntNps (a), Ag@AntNps (b, c), and Au@AntNps (d)

In this sense, multi-core and uncovered nanoparticles should not occur in samples with lower concentration of metal nanoparticles. Therefore, the AFM images reinforced the hypothesis that the smaller average size of AntNps obtained in the presence of AgNps or AuNps were related to the formation of hybrid Au@AntNp and Ag@AntNp core-shell structures.

After we confirmed that we obtained AntNps and hybrid core-shell structures for Ag@AntNPs and Au@AntNps, we investigated the fluorescence properties of these nanoparticles because the plasmon properties of metal nanoparticles can lead to metal-enhanced fluorescence (MEF) of the anthracene layer[39,1, 68,73,41,42], allowing for multiple applications in the biomedical field. According to the literature, MEF results from collective oscillation of free electron, or plasmons, by two mechanisms[39]. In the first mechanism, free electrons of metal nanoparticles and light waves interact strongly in resonant condition. As light propagates through the metal nanoparticle, free electrons collectively oscillate according to the electric field of the light. This is known as plasmon resonance and causes incident light to be absorbed or scattered, or both. This generates a plasmon band that can be

detected by UV-vis spectroscopy[38,39]. Plasmon resonance increases the local electric field, which enhances the excitation of the luminophore near the metal nanoparticles and hence its light emission[41,42]. This mechanism requires that the excitation spectrum of the luminophore and the plasmon band of the metallic nanoparticle be partially or totally overlapped.[38]

The second mechanism (mechanism 2) entails energy transfer from the luminophore in the excited state to the plasmon in the metal nanoparticles[41], resembling a Forster Resonant Energy Transfer. This demands that the emission spectrum of the luminophore and the plasmon band of the metallic nanoparticle be partially or completely overlapped[39,42]. On the basis of Figures 9a and b, the AntNp absorption and fluorescence spectra overlapped with the AgNp and AuNp plasmon bands, respectively. The AntNp fluorescence spectrum completely overlapped with the AgNp plasmon band, but it only partially overlapped with the AuNp plasmon band. Because MEF requires that the plasmon band overlap with the AntNp absorption or fluorescence spectrum, or both, enhancement was higher for Ag@AntNps compared to Au@AntNps. The anthracene fluorescence spectrum displays at least six peaks, around 380, 400, 42, 455, 495, and 532 nm (Figure 9a). By fixing the emission at 400 nm, the AntNp excitation spectrum presents three main peaks, at 250, 355, and 375 nm (Figure 9c). Thus, we selected these wavelengths as excitation wavelength for further experiments.

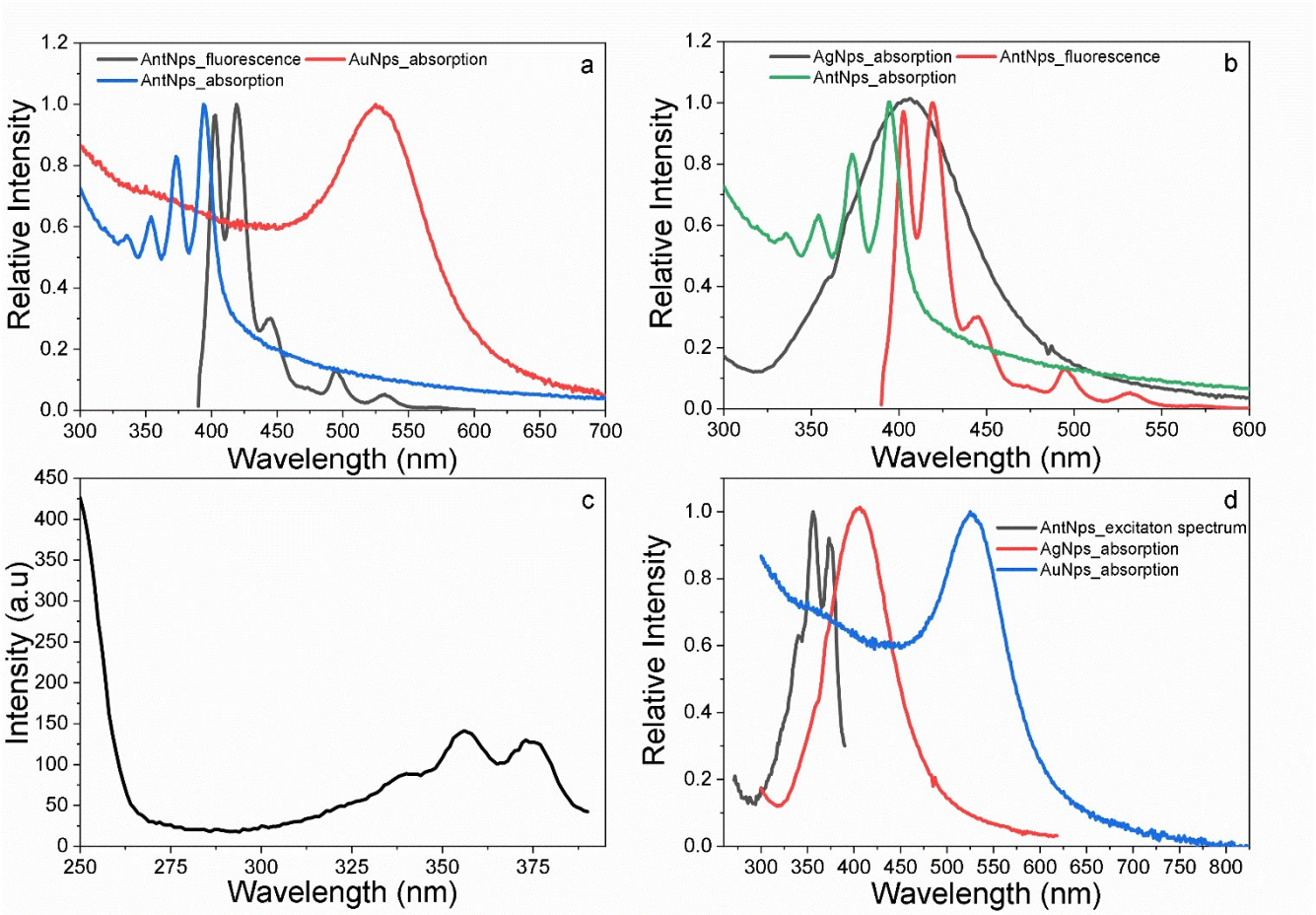

Figure 9 - Normalized absorption and fluorescence spectra of AntNps with AuNp (a) and AgNp (b) plasmon bands. Excitation spectrum of AntNps (c) and normalized \ excitation spectrum of AntNps with AgNp and AuNp absorption bands (d).

Figure 9d depicts the overlap between the anthracene excitation spectrum and the AgNp and AuNp plasmon bands, revealing greater overlap for AgNps than for AuNps. This result suggested that AgNps were more likely to cause plasmon-enhanced fluorescence. Interestingly, the excitation wavelengths of 375 and 355 nm coincided partially with the AgNp and AuNp plasmon bands, but the excitation wavelength of 250 nm did not resonate with them. Furthermore, the excitation wavelength of 355 nm partially resonated with the AgNp plasmon oscillation, whereas the excitation wavelength of 375 nm was close to the peak of the AgNp plasmon band (which is around 390 nm). Therefore, we expected that fluorescence enhancement would be more pronounced upon increasing excitation wavelength; that is, fluorescence enhancement should be higher for the excitation wavelength of 375 nm, followed by 355 nm and then 250 nm.

To confirm these analyses, we measured the fluorescence of several samples containing different AgNp or AuNp concentrations. Figures 10a, b, and c and Figures 11a, b, and c show the fluorescence spectra of Ag@AntNps and Au@AntNps, respectively, at three excitation wavelengths—250, 350, and 375 nm—as discussed previously. The presence of AgNps or AuNps intensified the fluorescence

intensity due to metal-enhanced fluorescence[37]. For the three excitation wavelengths (250, 355, and 375 nm), we calculated the fluorescence enhancement factor by dividing the fluorescence intensity of each emission peak of Ag@AntNps or Au@AntNps by the fluorescence intensity of each emission peak of AntNps. Fluorescence enhanced by up to 3.7-fold for Ag@AntNps (Figures 10f and i) and 1.5-fold for Au@AntNps (Figures 11f and i). Maximum enhancement was achieved for 0.08 mmol L^{-1} Ag@AntNps and 0.2 mol L^{-1} Au@AntNps. For concentrations above 0.08 mol L^{-1} Ag@AntNps, the fluorescence intensity was quenched, but it was still more intense than AntNp fluorescence and could be related to self-absorption of light due to the high AgNp or AuNp concentration.

We obtained the enhancements illustrated in Figures 10 and 11 by diluting AntNps, Ag@AntNPs, or Au@AntNPs 100 times in water. The enhancement factor was inversely related to the concentration: the higher the concentration, the lower the enhancement. This concentration-dependent enhancement stemmed from high concentrations of anthracene, the luminophore, and AgNps or AuNps, which resulted in various interactions, including radiative and non-radiative transfer and excimer formation, leading to quenching[30]. Moreover, if the sample was too concentrated, all the excitation light could be absorbed by the surface facing the light source, promoting primary and secondary inner-filter effects that further decreased fluorescence intensity[30,74].

We plotted fluorescence enhancement as a function of AgNp concentration (Figures 10d, e, and f). The emission peak around 400 nm enhanced for Ag@AntNps. This peak coincided with the maximum intensity of the AgNp plasmon band. Moreover, fluorescence enhancement clearly depended on the excitation wavelength: enhancement was higher for excitation at 375 nm (3.7-fold), followed by 355 (2.9-fold) and 250 nm (2.3-fold). These results reinforced the MEF hypothesis (mechanism 1) that higher enhancements are observed for wavelengths approaching the plasmon resonance peak[75,42]. Au@AntNPs also had a similar dependence on the excitation wavelength.

However, the enhancement factor was the same for all the anthracene bands ($\lesssim 1.5\ fold$), given the uncertainties. In other words, the enhancement for the band at 400 nm was not considerably higher than the enhancement for the other bands because the AuNp plasmon band (~510 nm) did not match any of these emission wavelengths. The highest enhancement factor for Au@AntNps was 1.5 $fold$,

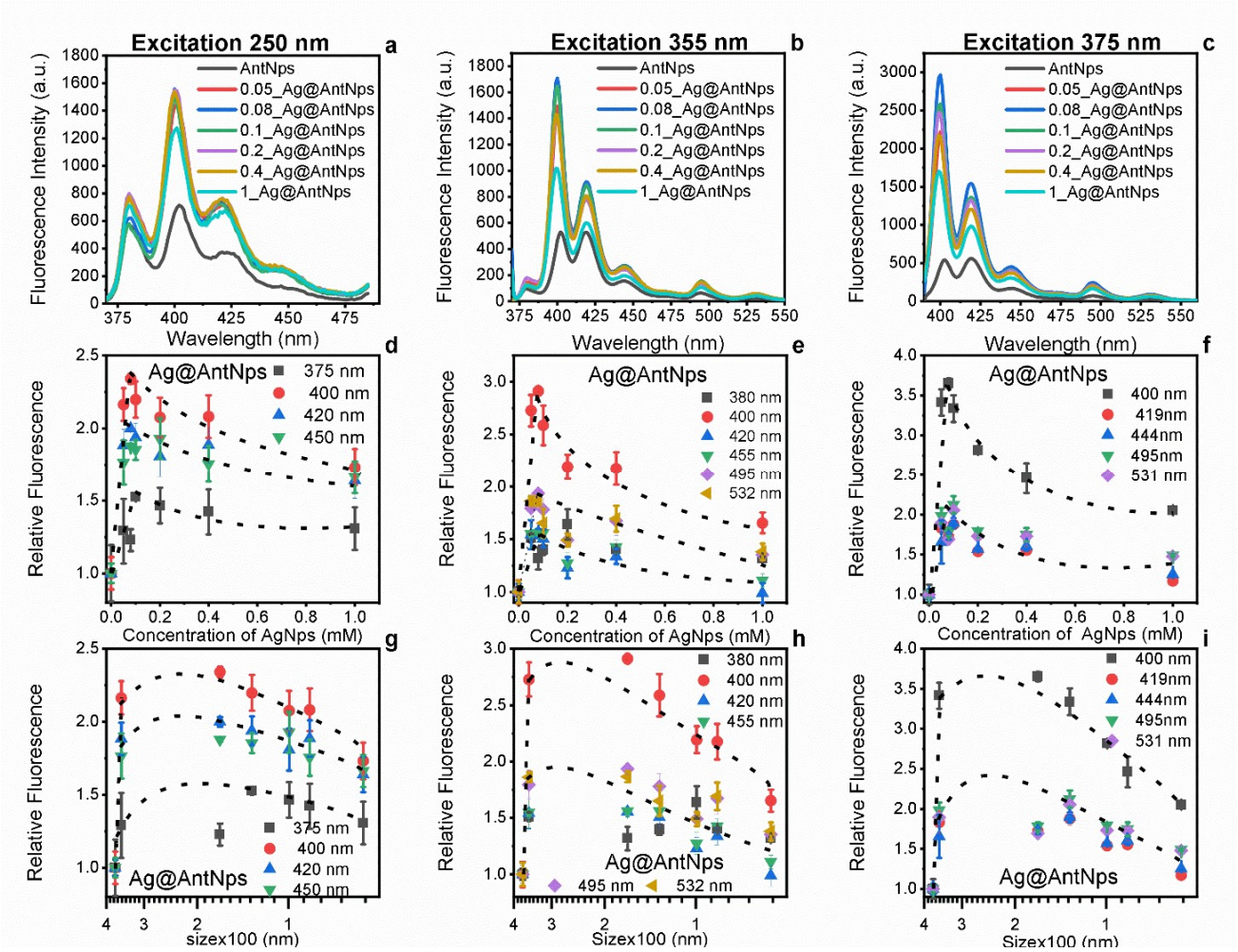

Figure 10 - Fluorescence intensities of AntNps and Ag@AntNps for several AgNp concentrations (mmol L-1) and at excitation wavelength of 250 (a), 355 (b), or 375 nm (c). Relative Fluorescence Enhancement at the same excitation wavelengths as a function of AgNp con centration (d), (e), (f) and nanoparticle size (g), (h), (i).

which was much smaller than the enhancements observed for Ag@AntNps. This finding was due to better overlap of the AgNp plasmon band with the anthracene emission and excitation spectra. This result reinforced the hypothesis of plasmon-enhanced fluorescence and evidenced the superior ability of AgNps to enhance anthracene fluorescence emission as compared to AuNps.

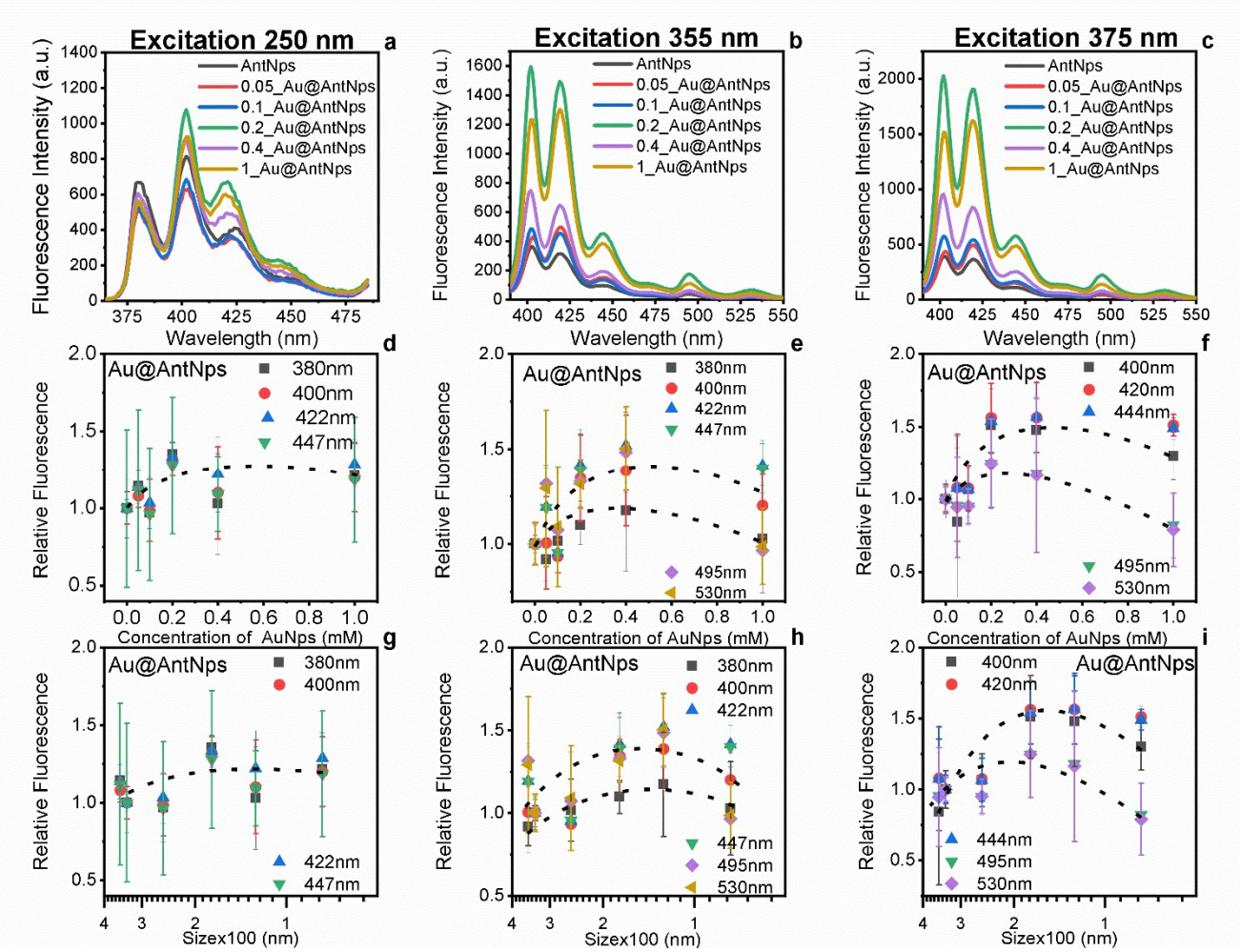

Figure 11 - Fluorescence intensities of AntNps and Au@AntNps for several AuNp concentrations (mmol L-1) at excitation wavelength of 250 nm (a), 355 (b), or 375 nm (c). Relative Fluorescence Enhancement at the same excitation wavelengths as a function of AuNp co concentration (d), (e), (f) and nanoparticle size (g), (h), (i)

DLS measurements revealed that the size of Ag@AntNps and Au@AntNps varied as a function of AgNp or AuNp concentration during the synthesis. Therefore, we had to verify if any size-effect took place by analyzing fluorescence enhancement as a function of particle size (Figures 10 and 11g, h, and i). Larger Ag@AntNps and Au@AntNps presented higher fluorescence enhancements compared to the smaller ones, but this phenomenon was more noticeable for Ag@AntNps due to higher fluorescence enhancement, as discussed previously. For Ag@AntNps, enhancement increased as particle size augmented, so that maximum enhancement (3.7-fold) occurred for an Ag@AntNp particle size of 164 nm (0.08 mol L^{-1}Ag@AntNps, Figure 10i). Further increase in AgNp concentration reduced the size of Ag@AntNps (Figure 7), diminishing, but still allowing fluorescence enhancement.

One possible explanation for this phenomenon is the combination of plasmon-enhancement and a size-dependent quenching mechanism. According to the literature, the main quenching mechanism for anthracene is Photoinduced Electron Transfer[30],[76] in which electron transfer from a luminophore to a

quencher suppresses fluorescence [39,30,77]. In this case, the orbital arrangement of the luminophore and the quencher must be favorable, resulting in overlapped orbitals even if the donor and acceptor are independent compounds and can move freely in the solution. However, quenching is more efficient upon contact between them, and binding must benefit orbital overlap.[39] Aromatic and aliphatic amines are well known for quenching most aromatic unsubstituted compounds; diethylaniline is considered the main quencher. Together with halogens, iodide, and thiocyanate, diethylaniline can efficiently suppress anthracene fluorescence.[30]

Although none of the aforementioned compounds were present in our samples, AgNps or AuNps could also act as quencher in Ag@AntNps or Au@AntNps, respectively, [73,78] and suppress fluorescence upon direct contact with anthracene molecules[78,73]. In fact, fluorescence quenching due to charge transfer has been observed for distances between the luminophore and the metal nanostructure shorter than 10 nm[39]. Here, the smaller size of Ag@AntNps and Au@AntNps and the thinner shell (once the size of the metal core does not change) allowed a larger amount of anthracene molecules to be closer to the quencher (metal surface). In this sense, the presence of an insulating layer between the metal core and the anthracene shell could have favored fluorescence enhancement. Besides that, molecular oxygen is well known for quenching fluorescence.[30] Given that Ag@AntNps and Au@AntNps were suspended in water, molecular oxygen should be abundant around them. As the size of Ag@AntNps and Au@AntNps decreased, the surface area increased, facilitating interaction between the outer anthracene layer and molecular oxygen in the medium, thereby suppressing fluorescence. These two hypotheses could be related to the smaller fluorescence enhancement observed for Ag@AntNps with AgNp concentration above 0.08 mmol L^{-1} (smaller size). If Ag@AntNps were too large (concentration below 0.08 mol L^{-1} Ag@AntNps), many anthracene molecules would be far enough from the metal core to prevent plasmon enhancement because enhancement factors decrease as a function of the distance between the luminophore and the metal nanoparticle[62,79–81] for distances above 10 nm. These might be the reasons why higher fluorescence enhancement was associated with an optimal size of the core-shell nanoparticles, around 100–150 nm.

The enhanced fluorescence intensity of the core-shell nanoparticles suggested that they could be used as energy mediators to induce $^1O_2$ generation by a PS. Here, we employed a TMTYP solution as PS to generate $^1O_2$.[82] The good overlap between anthracene fluorescence and TMTYP absorption, evidenced in Figure 12a, indicated that anthracene could be employed as energy mediator to excite the TMTYP molecules and hence generate $^1O_2$. To verify $^1O_2$ production, we used Electron Spin Resonance Spectroscopy (ESR) and employed TPC as spin-trap because it is specific for and sensitive to $^1O_2$ in a wide range of concentrations[26,53,83,66,51]. Upon TPC oxidation with $^1O_2$, a paramagnetic compound displaying three specific peaks in the ESR spectrum emerges[65,83]. Indeed, Mangkhalathon et al. detected

$^1O_2$ with TPC for several concentrations of a PS and showed that TPC works well even for low concentrations of PS.[84] Furthermore, TPC is stable, which allows $^1O_2$ to be quantified and detected several hours after irradiation[65].

Here, we selected 0.08 mol L^{-1} Ag@AntNps for the experiments because it provided higher fluorescence emission, and we used AntNps as control sample for comparative analyses. First, we mixed AntNps with 1 μmol L^{-1} TMTYP solution; then, we added 100 μmol L^{-1} TPC solution. Next, we irradiated the samples with visible light by using a band pass filter of 200–400 nm to ensure that only anthracene would be excited. In other words, $^1O_2$ should not be produced by direct excitation of the PS, so that any $^1O_2$ detected by ESR spectroscopy would result from the action of AntNps. To ensure that $^1O_2$ was not generated by direct TMTYP interaction with light, we conducted a control experiment under the same conditions, but we used only TMTYP and TPC solutions (without AntNps). Figure 12b shows that the ESR intensity (peak-to-peak amplitude) of TPC in the presence of TMTYP and AntNps after irradiation for 30 min was five times higher compared to TPC in the presence of TMTYP without AntNps, which confirmed that anthracene transferred energy to TMTYP and induced $^1O_2$ production. We monitored $^1O_2$ production for 60 min. Figure 6c illustrates the ESR intensity as a function of irradiation time, suggesting that $^1O_2$ generation increased linearly. The larger slope obtained for the TMTYP/AntNp solutions indicated that AntNps induced $^1O_2$ generation by TMTYP, so AntNps can be employed as energy mediator in photodynamic therapy (PDT).

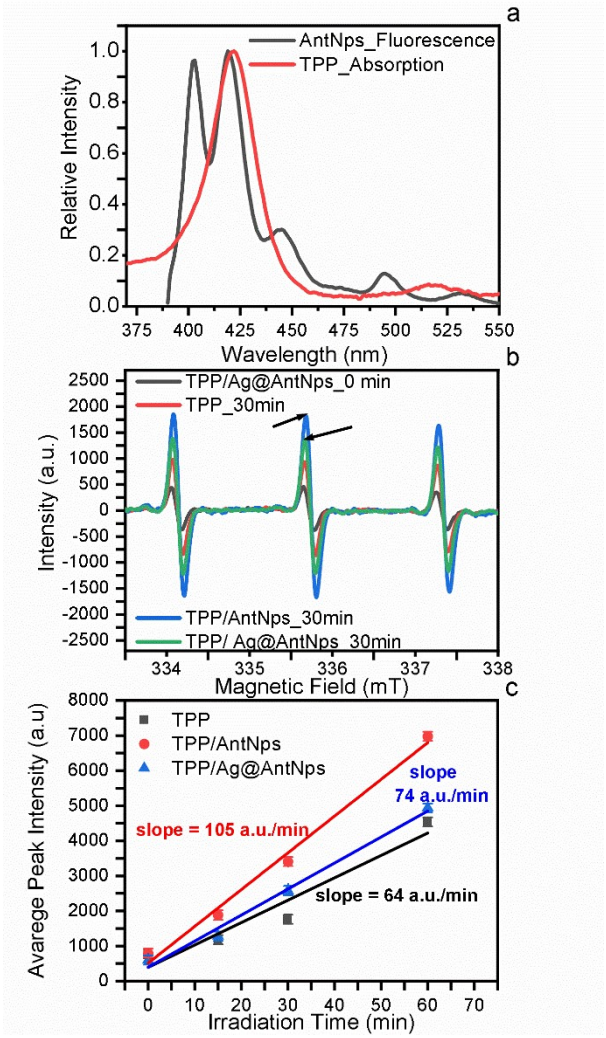

Figure 12 - (a) Overlap between normalized fluorescence of AntNps and normalized absorption of TMTYP. (b) ESR spectra of irradiated and non-irradiated TMTYP and of TMTYP/AntNps irradiated by using a band pass filter (200–400 nm). (c) ESR intensity versus irradiation time for Ag@AntNps (0.08 mmol L^{-1} Ag), TMTYP/AntNps, and TMTYP.

Given that AntNps proved potential energy mediators for application in PDT, 0.08 mol L^{-1} Ag@AntNps should generate more $^1O_2$ because they displayed higher fluorescence intensity, as depicted in Figures 12a and b. However, the ESR of TPC in the presence of TMTYP + 0.08 mol L^{-1} Ag@AntNps was less intense than the ESR of TPC in the presence of TMTYP + AntNps. As shown in Figure 12c, the slope obtained for TMTYP with 0.08 mol L^{-1} Ag@AntNps (74 a.u. min^{-1}) was smaller compared to AntNps (105 a.u min^{-1}). In a first moment, the fact that AntNps allowed 1.4-fold enhanced spin-trap detection of $^1O_2$ compared to 0.08 mol L^{-1} Ag@AntNps suggested that $^1O_2$ production was quenched instead of being enhanced because 0.08 mol L^{-1} Ag@AntNps had enhanced fluorescence.

We believe that the smaller detection of $^1O_2$ in the presence of the more fluorescent 0.08 mol L^{-1} Ag@AntNps could be related to anthracene molecules interacting more strongly with $^1O_2$ because these hybrid nanoparticles were smaller and consequently had larger surface area.

In fact, PAHs, like anthracene, may undergo photooxidation by trapping $^1O_2$ inside the aromatic ring (Figure 13), to give endoperoxides[60,85,86,87,88]. This reaction is characterized by loss of the optical properties (UV-vis absorption and fluorescence) of the PAH[66,85,89], so anthracene is also employed as probe to detect $^1O_2$ [86]. Therefore, when particle size decreased from ~400 nm in the case of AntNps to $\sim 100\ nm$ for 0.08 mol L^{-1} Ag@AntNps, the area/volume ratio increased by at least four-fold if we consider a smooth spherical surface. Given that the maximum fluorescence enhancement was 3.7-fold, larger surface interactions, which depend on the area/volume ratio, could counterbalance fluorescence enhancement. In other words, although fluorescence enhanced, the larger surface area could increase surface interactions/reactions with the surrounding medium, thereby decreasing the efficiency of $^1O_2$ production.

In this sense, the larger surface area of Ag@AntNps could increase the rate of endoperoxide formation, and surface anthracene molecules in Ag@AntNps could trap a significant quantity of generated $^1O_2$. In other words, anthracene irradiation and the consequent fluorescence emission could excite the PS, producing $^1O_2$. However, surface anthracene molecules could capture the as-generated $^1O_2$. Besides removing Singlet Oxygen from the medium, the endoperoxide resulting from the $^1O_2$-Ant reaction would no longer be able to induce $^1O_2$ generation because its fluorescence would be suppressed[86]. Therefore, the spin-trap would no longer detect $^1O_2$ because of the competing capture of the as-generated $^1O_2$ by anthracene and of fluorescence suppression. This could explain the lower $^1O_2$ detection in the case of 0.08 mol L^{-1} Ag@AntNps suggested by the TPC/ESR experiments. Even though this is not desirable, if one intends to use Ag@AntNps to generate $^1O_2$, these nanoparticles could be employed as carriers to deliver $^1O_2$ directly at the target tissue, from where the trapped $^1O_2$ could be released by thermal or optical stimulation.[60,85]

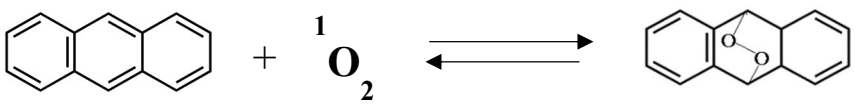

Figure 13 - Reversible binding between $^1O_2$ and anthracene, to form endoperoxide.

To verify whether anthracene captured $^1O_2$ in our nano systems, we investigated how AntNps and Ag@AntNps interacted with $^1O_2$. To this end, we mixed an aqueous 1 μmol L^{-1} TMTYP solution with 4 mmol L^{-1}AntNps and irradiated the resulting solution with UV-vis light. To ensure that only TTP was excited, we employed a band-pass filter of 400–600 nm. In fact, PAH can release trapped $^1O_2$ upon excitation with light of wavelength below 400 nm[60]. We performed the same experiment by using 0.08 mol L^{-1} Ag@AntNps (higher fluorescence intensity) or 1 mol L^{-1} Ag@AntNps (larger surface area/ smaller size). During irradiation with UV-vis light, we recorded the fluorescence spectra of

TMTYP/AntNps and TMTYP/Ag@AntNPs as a function of exposure time. Figure 14 depicts fluorescence quenching as a function of irradiation time. The Figure indicates the aforementioned reaction with $^1O_2$ and consequent endoperoxide formation, as reported in the literature[60,86].

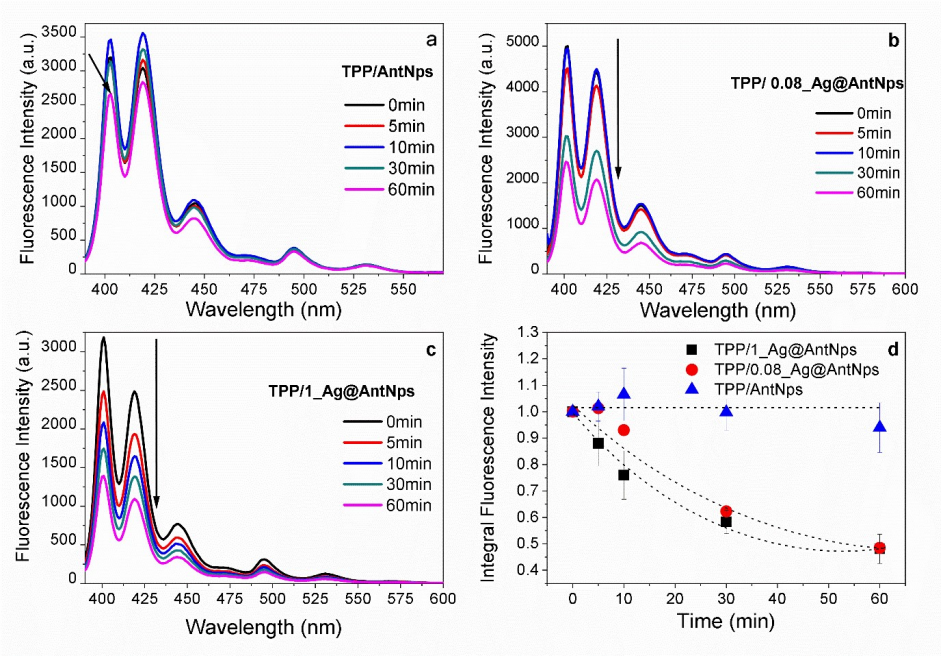

Figure 14 - Fluorescence spectrum of TMTYP/AntNps (a), TMTYP/0.08 mol L^{-1} Ag@AntNps (b), and TMTYP/1 mol L^{-1} Ag@AntNps (c) irradiated with light in the range of 400–580 nm; a pass band filter was used for $^1O_2$ trapping, leading to loss of AntNp fluorescence. Normalized area integrated under the fluorescence curve for each sample, irradiated for 60 min (d).

As discussed previously, smaller nanoparticles present larger surface area, which provides more contact with molecular species in the medium. In this case, the quenching caused by $^1O_2$ should be more noticeable compared to bigger nanoparticles. In other words, compared to larger nanoparticles such as AntNps, endoperoxide formation (characterized by anthracene fluorescence quenching) should be faster in smaller nanoparticles like 1 mol L^{-1} Ag@AntNps because more anthracene molecules would be in direct contact with $^1O_2$ generated by TMTYP. Figure 14d shows that, after irradiation for 60 min, the fluorescence intensity (total spectrum area) of 1 mol L^{-1} Ag@AntNps decreased by half (48%), whereas the intensity of AntNps decreased by only 6% (relative intensities decreased from 1.0 to 0.94). Given that both samples had the same concentration of anthracene, this result suggested that AntNps barely absorbed $^1O_2$ from the medium, or that the quantity of trapped $^1O_2$ did not suffice to quench fluorescence significantly because AntNps had larger diameters. In contrast, Ag@AntNps captured 8-fold more $^1O_2$ than AntNps. Taking this into account and considering that the spin-trap detection of $^1O_2$ by AntNps was only 1.4-fold higher than by Ag@AntNps (Figure 12c), we inferred that the overall $^1O_2$ production; that is, $^1O_2$ captured by spin-trap + $^1O_2$ captured by surface anthracene molecules, was in fact higher for Ag@AntNps, as expected from their higher fluorescence emission.

Compared to AntNps, fluorescence intensity decayed faster for 1 mol L^{-1} Ag@AntNps and 0.08 mol L^{-1} Ag@AntNps. Given that Ag@AntNps were smaller than AntNps (Figure 7), this result confirmed that Ag@AntNps interacted more with quenchers ($^1O_2$) in the medium. Enhanced loading of $^1O_2$ in Ag@AntNps could be useful for controlled delivery of ROS in cancer therapy, for instance, and suggested that Ag@AntNps had faster and superior $^1O_2$ loading capacity. In other words, this result revealed that Ag@AntNps could be suitable carriers of $^1O_2$ produced ex-situ.

Such remarkable quenching of Ag@AntNps fluorescence in the presence of $^1O_2$ could also be related to plasmon-enhanced fluorescence caused by the metal core. Because the presence of $^1O_2$ species was estimated in terms of fluorescence intensity, and since anthracene fluorescence was enhanced via plasmon interaction, if a small number of anthracene molecules were quenched by reaction with $^1O_2$, this would decrease the fluorescence intensity more significantly for the plasmonic Ag@AntNPs than for AntNps. In other words, Ag@AntNps would be more sensitive for $^1O_2$ detection in aqueous medium due to plasmon-enhanced fluorescence, suggesting that they could be employed as more sensitive $^1O_2$ fluorescent probes while also carrying $^1O_2$. Figure 8d evidenced that AntNps were not a suitable $^1O_2$ probe: their large size and the absence of plasmonic interaction prevented fluorescence from being quenched in the experimental conditions. Therefore, the smaller size and plasmon-enhanced fluorescence of Ag@AntNps make them new potential $^1O_2$ fluorescent probes with plasmon-enhanced sensitivity.

Given that anthracene has scintillation properties, we verified whether it also acted as energy mediator upon excitation with X-rays. Figure 15a shows the radioluminescence spectra of AntNps and Ag@AntNps. Under X-rays, light was emitted in the same range as compared to AntNp fluorescence, suggesting that energy transfer between anthracene and TMTYP should also take place upon excitation with X-rays. In this sense, we irradiated AntNps or Ag@AntNps mixed with TMTYP with X-rays in the presence of the spin-trap TPC and performed ESR measurements to investigate $^1O_2$ production. Figure 15b depicts the ESR intensity as a function of X-ray dose for samples containing only TPC, TPC+TMTYP, TPC+TMTYP+AntNps, or TPC+TMTYP+Ag@AntNPs. Although TPC is extensively used to probe $^1O_2$ produced under UV-visible irradiation, Figure 15b revealed that TPC alone exhibited ESR signal upon irradiation with X-rays. The presence of TMTYP along with TPC did not intensify the ESR signal, revealing that the X-rays did not excite TMTYP. However, the presence of an ESR signal for TPC alone suggested that X-rays could damage TPC, or that another mechanism for $^1O_2$ generation under irradiation with X-rays could take place. Similar sensitization of a green sensor that is widely used to probe $^1O_2$ has been verified upon irradiation with X-rays.[90]

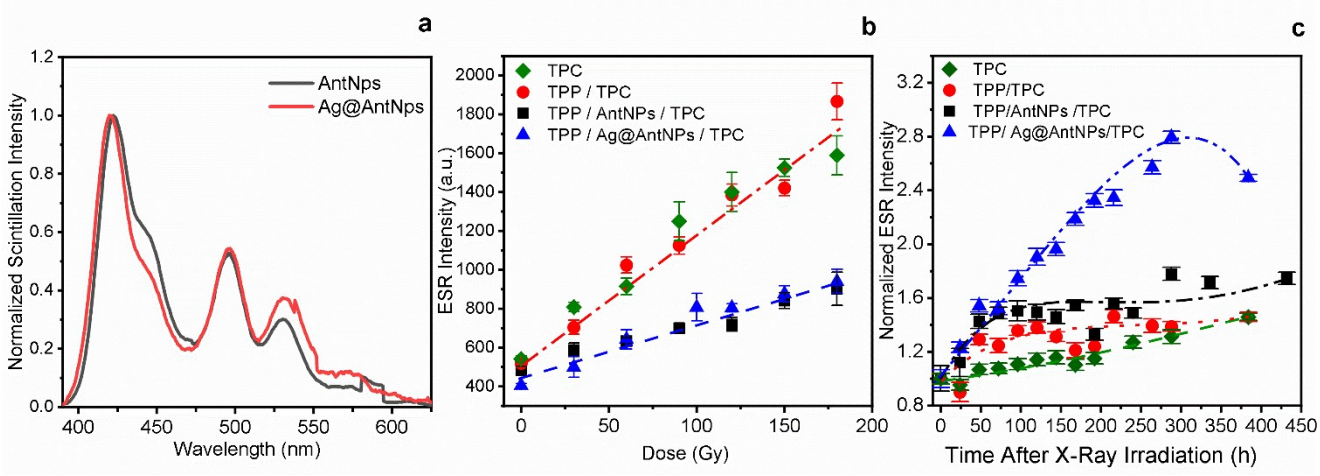

Figure 15 - AntNps and Ag@AntNps radiofluorescence (a) arithmetic mean of the three ESR peaks after irradiation of the control samples (TPC, TMTYP/TPC) and porphyrin solution plus nanoparticles (TMTYP/AntNps/TPC and TMTYP/Ag@AntNps/TPC) with cumulative doses of X-rays for $^1O_2$ generation; and (b) arithmetic mean of the three ESR peaks of the irradiated samples – spin marker added after irradiation – for two weeks to investigate $^1O_2$ release.

In fact, $^1O_2$ generation in water under sonication and in the presence of dissolved molecular oxygen has been reported; TPC was used as spin trap, and ESR measurements were accomplished.[91] A mechanism for $^1O_2$ production under sonication was proposed: sonication of water generates HO· (hydroxyl) and H· radicals[91]. Then, if molecular oxygen (O_2) is present, the HO· radical interacts with O_2, to form HOOO·, which is converted to HO· and $^1O_2$ see Figure 16. Dissolved O_2 and HO· were also present in our samples during irradiation with X-rays[92]. More specifically, upon irradiation with X-rays, water molecules were ionized, to generate several radicals, including the extremely reactive HO·[92]. The resulting HO· interacted with O_2, to afford $^1O_2$ in a mechanism resembling the mechanism proposed in Figure 10. Furthermore, according to the literature, if dissolved O_2 is present in water during irradiation with X-rays, O_2 reduction produces superoxide radicals, which are precursors of $^1O_2$ and other ROS.[92] Therefore, we attributed the ESR signal of the control samples irradiated with X-rays to TPC oxidation by $^1O_2$ generated as a sub-product of water radiolysis in the presence of dissolved O_2.

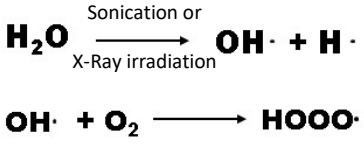

Figure 16 - Schematic illustration of 1O2 generation in sonicated water/water irradiated with X-rays in the presence of dissolved molecular oxygen. Adapted from [94]

Although we expected that anthracene scintillation would produce $^1O_2$, Figure 15b revealed less intense TPC ESR for AntNps and Ag@AntNps. Given that anthracene can also scavenge $^1O_2$, $^1O_2$ capture by anthracene prevailed over anthracene scintillation-induced $^1O_2$ production. Generation of $^1O_2$ as a sub-product of water radiolysis was more likely because X-rays interacted with water molecules rather than AntNps and Ag@AntNps—water was the most abundant component in our samples. In this case, anthracene captured the produced $^1O_2$.

AntNps and Ag@AntNps inhibited TPC oxidation to the same extent, even 0.08 mol L^{-1} Ag@AntNPs, which had smaller size and larger surface area. We had expected that the larger surface area of Ag@AntNps would result in less TPC oxidation compared to AntNps, unless Ag@AntNps induced higher overall $^1O_2$ generation than AntNps, as observed upon irradiation with light. To verify whether AntNps and Ag@AntNps would release $^1O_2$, we monitored the ESR intensity of samples with AntNps and Ag@AntNps until their ESR signals stopped increasing. If endoperoxide emerged during irradiation with X-rays, $^1O_2$ would be released within a few hours upon optical or thermal stimulation[60, 93], or within several hours up to days or months if the samples were kept in the dark and at room temperature[60, 93], depending on the endoperoxide half-life. Because the half-life of anthracene endoperoxide has never been reported and the half-life of dissolved anthracene molecules may differ from the half-life of solid AntNps, we kept all the irradiated samples in the dark and at room temperature for several days and monitored the ESR intensity of the spin-trap, so that any intensification during this period would indicate that the trapped $^1O_2$ was released.

Figure 15c shows that the ESR intensity of TPC irradiated with X-rays increased slowly and linearly as a function of time. The maximum increase of 46% was reached 18 days after irradiation, whereas the ESR intensity of TPC+TMTYP increased ~20% within the first 48 h after irradiation, but it reached a plateau around this value thereafter. The ESR intensity of the irradiated sample containing AntNps increased around 50% in the first 48 h, and then it slowly increased to a maximum of 77% enhancement up to day 12. However, the ESR intensity of Ag@AntNps irradiated with X-rays increased more significantly and faster, with maximum enhancement of 180% 12 days post-irradiation. Considering the same post-irradiation period of 12 days, the ESR intensity of TPC, TPC+TMTYP, and TPC+TMTYP +AntNps increased by 31%, 38%, and 77%, respectively, which were much lower than the 180% observed for TPC+TMTYP+Ag@AntNps. Because the quantity of $^1O_2$ that was released by Ag@AntNps was more than twice the amount released by AntNPs, this result agreed with the hypothesis that $^1O_2$ production upon irradiation with X-rays was higher for Ag@AntNps.

Therefore, our findings suggest that Ag@AntNps induced higher overall $^1O_2$ generation in the medium upon irradiation with visible light or X-rays, but the spin-trap captured only a small part of the generated $^1O_2$ because the surface anthracene molecules competed for $^1O_2$. In other words, the presence

of the metal core in Ag@AntNps not only increased the efficiency of $^1O_2$ production upon irradiation with visible light or X-rays due to plasmon-enhanced fluorescence, but it also improved the ability of the AntNps to capture and to store the as-generated $^1O_2$. This happened thanks to the higher surface-to-volume ratio of Ag@AntNps, which promoted sustained $^1O_2$ release for up to 12 days after irradiation. This could be an interesting approach to extend the radiation therapy treatment after the irradiation sessions, a phenomenon that has never been reported.

Besides plasmon-enhanced fluorescence, another possible reason for the higher overall $^1O_2$ generation was the high atomic number (Z) of the metal core in the hybrid core-shell nanoparticles, which enhanced the dose delivered to the surroundings (anthracene layer and water), thereby increasing $^1O_2$ production. Insertion of materials with high Z in the tumoral region enhances the interaction of X-rays within the tumor because the mass absorption coefficient of the loaded tumor region increases[61, 50, 94]. Upon interaction with X-rays of appropriate energy, electrons are ejected from the metal nanoparticles, increasing the radiation dose delivered to the surrounding medium. For instance, the use of AuNps in RT treatment increases the survival rates of cancer-bearing mice by 66% compared to RT treatment without AuNps.[47]

Thus, the presence of AgNps and AuNps in Ag@AntNps and Au@AntNps, respectively, could increase the interaction between the X-rays and the anthracene layer, and between the X-rays and water in the medium, thereby increasing the delivered dose. Although several works have already demonstrated that AgNps and AuNps can lead to dose enhancement, the presence of a thick anthracene shell could attenuate the electrons ejected by the metal core, decreasing the dose delivered to the medium. To investigate whether the core-shell structure of metal@AntNps allows for dose enhancement, we mixed 1 mol L^{-1} Au@Ant with alanine powders and irradiated them with different X-ray doses. Alanine is a reference dosimetric material because it is tissue-equivalent; i.e., ionizing radiation interacts with alanine in a similar way that this radiation interacts with soft biological tissues[49]. Moreover, interaction with ionizing radiation produces stable free radicals, which can be detected by ESR spectroscopy.[49] In this sense, comparing the ESR intensity of pure alanine with the ESR intensity of alanine containing materials with high Z is a powerful method to infer about the dose enhancement factor (DEF) prompted by the nanoparticles[50,51]. The DEF can be calculated by considering the quotient between the peak-to-peak amplitude of the central line of the ESR spectra of the samples (Figure 11a) with and without Au@AntNps.[50]

Figure 17a displays the Ala and Ala_Au@AntNp ESR spectra irradiated with 60 Gy. The ESR intensity of Ala_Au@AntNps was more intense than the ESR intensity of Ala. Figure 17b depicts the dose-response curve for samples irradiated with cumulative doses from 10 Gy to 60 Gy. Both curves indicated that the production of radiation-induced free-radicals was higher in Ala_Au@AntNps,

revealing that the anthracene layer around the Au core did not attenuate all the electrons ejected by the metal. The DEF based on the ratio between the slopes of the dose-response curves of Ala and Ala_Au@AntNps was 1.49; that is, the radiation dose delivered to the alanine molecules increased by 49% in the latter case. Therefore, the metal core in Ala_Au@AntNps could increase the interaction between X-rays and soft tissues (represented by alanine), which could enhance radiosensitization by either local dose enhancement or enhanced generation/release of ROS. In conclusion, Ag@AntNps and Au@AntNp have potential application in combined RT and PDT their metal core can enhance the delivered radiation dose besides delivering $^1O_2$ when a previous load of ROS is administered and/or by inducing in-situ $^1O_2$ production if administrated unloaded (or after releasing $^1O_2$ and recovering fluorescence) conjugated to a PS.

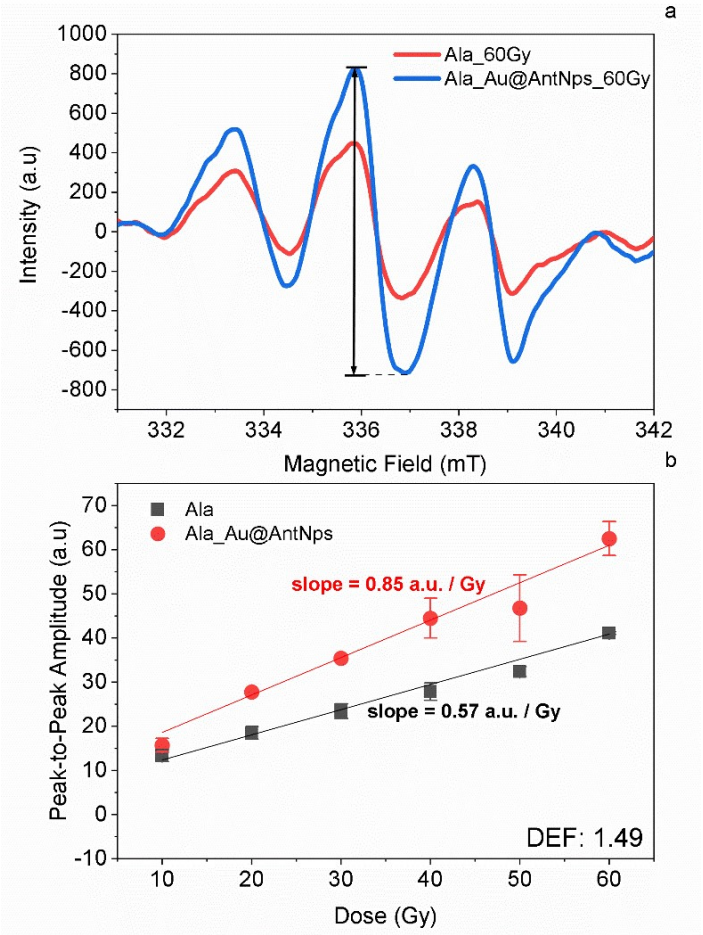

Figure 17 (a) ESR spectrum of pure Alanine (Ala) and Alanine containing Au@AntNps (1%wt) (Ala_Au@AntNps) for samples irradiated with 60 Gy and 80 keV (effective energy 48 keV), and (b) central line peak-to-peak amplitude of the ESR spectrum. Error bars refer to the standard deviation from three different samples. DEF was calculated by considering the ratio between the slope of the linear fit for Ala_Au@AntNps and the control Ala.

5. *Conclusion*

We successfully synthesized anthracene and metal@anthracene nanoparticles. The presence of the metal nanoparticles (AgNps or AuNps) during the synthesis of AntNps reduced the hydrodynamic radius of the AntNps due to formation of a core-shell nanostructure, as confirmed by AFM images. We investigated the optical properties of AntNps, Ag@AntNPs, and Au@AntNps and attributed the enhanced fluorescence of Ag@AntNPs, and Au@AntNps to coupling with localized surface plasmons, which promoted plasmon-enhanced fluorescence. AgNps allowed for larger fluorescence enhancements because the AgNp plasmon resonance overlapped better with the anthracene fluorescence spectrum. Fluorescence enhanced for all the AgNp concentrations. Fluorescence enhancement depended on the metal nanoparticle concentration and the core-shell size. The stronger emission observed for the larger hybrid nanoparticles, compared to the smaller ones, was due to the larger surface area of the small nanoparticles, which increased the contact between surface anthracene molecules and quenchers in the medium.

AntNps and Ag@AntNps acted as energy mediators during $^1O_2$ generation under irradiation with UV-vis light. $^1O_2$ detection by the ESR spin-trap in the presence Ag@AntNps or Au@AntNps was counterbalanced by their increased surface area and consequent higher $^1O_2$ capture rate. However, together, the ESR and fluorescence results suggested that the overall production of $^1O_2$ ($^1O_2$ captured by spin-trap + $^1O_2$ captured by surface anthracene molecules) was higher for Ag@AntNps than for AntNps. Thanks to plasmon-enhanced fluorescence and increased surface area, Ag@AntNps stood out as a new and more sensitive fluorescent $^1O_2$ probe. During irradiation with X-rays, AntNps and Ag@AntNps scavenged $^1O_2$ and stored most $^1O_2$produced during irradiation. The trapped $^1O_2$ were later released, bringing about sustained $^1O_2$ release for up to 12 days after irradiation. This could be an interesting approach to extend the radiation therapy treatment after the irradiation sessions, which has never been reported. Furthermore, the presence of the metal nanoparticle in the core of the hybrid core-shell nanostructures increased the interaction with X-rays, leading to radiation dose enhancement around the nanoparticle. To sum up, metal/anthracene nanostructures are a potential platform for combining radiation and photodynamic therapies. Depending on the nanoparticle configuration, different approaches can be used to combine RT and PDT, and the AntNps, Ag@AntNps and Au@AntNps should be carefully designed to achieve the desired properties.

6. References

1. Guidelli, E. J., Ramos, A. P. & Baffa, O. Silver nanoparticle films for metal enhanced luminescence: Toward development of plasmonic radiation detectors for medical applications. *Sensors Actuators, B Chem.* **224**, 248–255 (2016).

2. Resende L. P.; Rothberg D., S. C. M. Inovação, Estudos CTS e Comunicação Científica: A divulgação das pesquisas de materiais cerâmicos e nanotecnologia. (Universidade Federal de São Carlos, 2011).

3. Long, N. V. *et al.* Biomedical applications of advanced multifunctional magnetic nanoparticles. *J. Nanosci. Nanotechnol.* **15**, 10091–10107 (2015).

4. Notarianni, M. *et al.* Plasmonic effect of gold nanoparticles in organic solar cells. *Sol. Energy* **106**, 23–37 (2014).

5. Balling, P. *et al.* Improving the efficiency of solar cells by upconverting sunlight using field enhancement from optimized nano structures. *Opt. Mater. (Amst).* **83**, 279–289 (2018).

6. Patanjali, P., Singh, R., Kumar, A. & Chaudhary, P. Nanotechnology for water treatment: A green approach. in *Green Synthesis, Characterization and Applications of Nanoparticles* 485–512 (Elsevier, 2019). doi:10.1016/b978-0-08-102579-6.00021-6.

7. Gehrke, I., Geiser, A. & Somborn-Schulz, A. Innovations in nanotechnology for water treatment. *Nanotechnology, Science and Applications* vol. 8 1 (2015).

8. De, V. & Teixeira, C. Síntese e Caracterização de Cintiladores de Aluminossilicatos nanoestruturados, dopados com Ce 3+, Eu3+ e Mn 2+. (Universidade Federal de Sergipe, 2014).

9. Siegel, R. L., Miller, K. D. & Jemal, A. Cancer statistics, 2020. *CA. Cancer J. Clin.* **70**, 7–30 (2020).

10. de Almeida, E. M., Ferreira, H. J., Alves, D. R. & da Silva, W. M. B. Therapeutic potential of medicinal plants indicated by the Brazilian public health system in treating the collateral effects induced by chemotherapy, radiotherapy, and chemoradiotherapy: A systematic review. *Complementary Therapies in Medicine* vol. 49 102293 (2020).

11. Long, N. V. *et al.* Biomedical applications of advanced multifunctional magnetic nanoparticles. *J. Nanosci. Nanotechnol.* **15**, 10091–10107 (2015).

12. Ren, X. D. *et al.* Progress in the development of nanosensitizers for X-ray-induced photodynamic therapy. *Drug Discovery Today* vol. 23 1791–1800 (2018).

13. Nurgali, K., Jagoe, R. T. & Abalo, R. Editorial: Adverse effects of cancer chemotherapy: Anything new to improve tolerance and reduce sequelae? *Frontiers in Pharmacology* vol. 9 (2018).

14. Taylor, C. *et al.* Estimating the Risks of Breast cancer radiotherapy: Evidence from modern radiation doses to the lungs and Heart and From previous randomized trials. *J. Clin. Oncol.* **35**, 1641–1649 (2017).

15. Procházková, L., Pelikánová, I. T., Mihóková, E., Dědic, R. & Čuba, V. Novel scintillating nanocomposite for X-ray induced photodynamic therapy. *Radiat. Meas.* **121**, 13–17 (2019).

16. Sengar, P. *et al.* Dualphotosensitizer coupled nanoscintillator capable of producing type I and type II ROS for next generation photodynamic therapy. *J. Colloid Interface Sci.* **536**, 586–597 (2019).

17. Wang, G. D. *et al.* X-ray induced photodynamic therapy: A combination of radiotherapy and photodynamic therapy. *Theranostics* **6**, 2295–2305 (2016).

18. Oliveira, K. T. de, Souza, J. M. de, Gobo, N. R. da S., Assis, F. F. de & Brocksom, T. J. Basic Concepts and Applications of Porphyrins, Chlorins and Phthalocyanines as Photosensitizers in Photonic Therapies. *Rev. Virtual Química* **7**, 310–335 (2015).

19. Kamkaew, A., Chen, F., Zhan, Y., Majewski, R. L. & Cai, W. Scintillating Nanoparticles as Energy Mediators for Enhanced Photodynamic Therapy. *ACS Nano* **10**, 3918–3935 (2016).

20. Wang, G. D. *et al.* X-ray induced photodynamic therapy: A combination of radiotherapy and photodynamic therapy. *Theranostics* **6**, 2295–2305 (2016).

21. Nyman, E. S. & Hynninen, P. H. Research advances in the use of tetrapyrrolic photosensitizers for photodynamic therapy. *J. Photochem. Photobiol. B Biol.* **73**, 1–28 (2004).

22. Castano, A. P., Demidova, T. N. & Hamblin, M. R. Mechanisms in photodynamic therapy: Part three - Photosensitizer pharmacokinetics, biodistribution, tumor localization and modes of tumor destruction. *Photodiagnosis and Photodynamic Therapy* vol. 2 91–106 (2005).

23. Ibanez Simplicio, F., Maionchi, F. & Hioka, N. Terapia fotodinâmica: Aspectos farmacológicos, aplicações e avanços recentes no desenvolvimento de medicamentos. *Quim. Nova* **25**, 801–807 (2002).

24. Lehninger;R, A. L; Nelson, D.L; Cox, M. M. (2000). Princípios de Bioquímica. São Paulo.Sarvier, São Paulo - Google Shopping.

25. Chen, X., Song, J., Chen, X. & Yang, H. X-ray-activated nanosystems for theranostic applications. *Chemical Society Reviews* vol. 48 (2019).

26. Okuno, E. & Yoshimura, E. *Física das Radiações*. (2010).

27. Desouky, O., Ding, N. & Zhou, G. Targeted and non-targeted effects of ionizing radiation. *J. Radiat. Res. Appl. Sci.* **8**, 247–254 (2015).

28. Chen, X., Song, J., Chen, X. & Yang, H. X-ray-activated nanosystems for theranostic applications. *Chem. Soc. Rev.* **48**, 3073–3101 (2019).

29. Principles, F. : & Valeur, A. B. *Bernard Valeur Molecular Fluorescence Principles and Applications*.

30. Lakowicz, J. R. *Principles of fluorescence spectroscopy*. *Principles of Fluorescence Spectroscopy* (2006). doi:10.1007/978-0-387-46312-4.

31. Mohammad A. Omary, H. H. P. *Encyclopedia of Spectroscopy and Spectrometrye*. (2017).

32. Waller, D. G., Omary, M. A. & Patterson, H. H. *Anthracenes Skin disorders Luminescence, Theory*. (2018).

33. Nikl, M. & Yoshikawa, A. Recent R&D Trends in Inorganic Single-Crystal Scintillator Materials for Radiation Detection. *Adv. Opt. Mater.* **3**, 463–481 (2015).

34. Knoll, G. E., Arbor, A. & Wiley, J. *Radiation Detectibn and Measurement Third Edition*. (2000).

35. Wang, C. *et al.* Synergistic assembly of heavy metal clusters and luminescent organic bridging ligands in metal-organic frameworks for highly efficient X-ray scintillation. *J. Am. Chem. Soc.* **136**, 6171–6174 (2014).

36. Lakowicz, J. R. Plasmonics in biology and plasmon-controlled fluorescence. *Plasmonics* vol. 1 5–33 (2006).

37. Lakowicz, J. R. *et al.* Plasmon-controlled fluorescence: A new paradigm in fluorescence spectroscopy. *Analyst* vol. 133 1308–1346 (2008).

38. Guidelli, E. J., Ramos, A. P. & Baffa, O. Optically Stimulated Luminescence Under Plasmon Resonance Conditions Enhances X-Ray Detection. *Plasmonics* **9**, 1049–1056 (2014).

39. Lakowicz, J. R. Radiative decay engineering 5: Metal-enhanced fluorescence and plasmon emission. *Anal. Biochem.* **337**, 171–194 (2005).

40. Guidelli, E. J., Ramos, A. P. & Baffa, O. Optically Stimulated Luminescence Under Plasmon Resonance Conditions Enhances X-Ray Detection. *Plasmonics* **9**, 1049–1056 (2014).

41. Park, J.-E., Kim, J. & Nam, J.-M. Emerging plasmonic nanostructures for controlling and enhancing photoluminescence. (2017) doi:10.1039/c7sc01441d.

42. Yu, H., Peng, Y., Yang, Y. & Li, Z. Y. Plasmon-enhanced light–matter interactions and applications. *npj Computational Materials* vol. 5 1–14 (2019).

43. *HANDBOOK FOR DOSE ENHANCEMENT EFFECTS IN ELECTRONIC DEVICES Air Force Systems Command*. (1983).

44. Roesk, J. C. (Universit. of C., Nunez, L. (Argonne N. L., Hoggarth, M. (DePaul U., Labay, E. (University of C. & Weichselbaum, R. R. (universit. of C. Characterization of the Theorectical Radiation Dose Enhancement from Nanoparticles. *Technol. Cancer Res. Treat.* **6**, 395–401 (2007).

45. Kakade, N. R. & Sharma, S. D. Dose enhancement in gold nanoparticle-aided radiotherapy for the therapeutic photon beams using Monte Carlo technique. *J. Cancer Res. Ther.* **11**, 94–97 (2015).

46. Guidelli, E. J. & Baffa, O. Influence of photon beam energy on the dose enhancement factor caused by gold and silver nanoparticles: An experimental approach. *Med. Phys.* **41**, (2014).

47. Hainfeld, J. F., Slatkin, D. N. & Smilowitz, H. M. The use of gold nanoparticles to enhance radiotherapy in mice. *Phys. Med. Biol.* **49**, (2004).

48. Guidelli, E. J., Ramos, A. P., Zaniquelli, M. E. D., Nicolucci, P. & Baffa, O. Synthesis and characterization of silver/alanine nanocomposites for radiation detection in medical applications: The influence of particle size on the detection properties. *Nanoscale* **4**, 2884–2893 (2012).

49. Guidelli, E. J., Ramos, A. P., Zaniquelli, M. E. D., Nicolucci, P. & Baffa, O. Synthesis and characterization of gold/alanine nanocomposites with potential properties for medical application as radiation sensors. *ACS Appl. Mater. Interfaces* **4**, 5844–5851 (2012).

50. Guidelli, E. J., Ramos, A. P., Zaniquelli, M. E. D., Nicolucci, P. & Baffa, O. Synthesis and characterization of gold/alanine nanocomposites with potential properties for medical

application as radiation sensors. *ACS Appl. Mater. Interfaces* **4**, 5844–51 (2012).

51. Guidelli, E. J. & Baffa, O. Influence of photon beam energy on the dose enhancement factor caused by gold and silver nanoparticles: An experimental approach. *Med. Phys.* **41**, 032101 (2014).

52. Bhopate, D. P., Mahajan, P. G., Garadkar, K. M., Kolekar, G. B. & Patil, S. R. Polyvinyl pyrrolidone capped fluorescent anthracene nanoparticles for sensing fluorescein sodium in aqueous solution and analytical application for ophthalmic samples. *Luminescence* **30**, 1055–1063 (2015).

53. Koh, E. & Fluhr, R. Singlet oxygen detection in biological systems: Uses and limitations. *Plant Signaling and Behavior* vol. 11 (2016).

54. Iwegbue, C. M. A. *et al.* Evaluation of Human Exposure to Polycyclic Aromatic Hydrocarbons from Some Edible Oils and Shea Butter in Nigeria. *Polycycl. Aromat. Compd.* 1–15 (2019) doi:10.1080/10406638.2019.1570951.

55. Hasue, F. M. *et al.* Assessment of genotoxicity and depuration of anthracene in the juvenile coastal fish Trachinotus carolinus using the comet assay. *Brazilian J. Oceanogr.* **61**, 215–222 (2013).

56. Sun, W., Zhou, Z., Pratx, G., Chen, X. & Chen, H. Nanoscintillator-mediated X-ray induced photodynamic therapy for deep-seated tumors: From concept to biomedical applications. *Theranostics* vol. 10 1296–1318 (2020).

57. Structure and Dynamics of Hemoglobin Subunits and of Myoglobin. 345–372 (2004) doi:10.1016/B978-044451449-3/50009-5.

58. Kottuparambil, S. & Park, J. Anthracene phytotoxicity in the freshwater flagellate alga Euglena agilis Carter. *Sci. Rep.* **9**, 1–11 (2019).

59. Padilla, R., Rodriguez-Corrales, J. A., Donohoe, L. E., Winkel, B. S. J. & Brewer, K. J. A new class of Ru(II) polyazine agents with potential for photodynamic therapy. *Chem. Commun.* **52**, 2705–2708 (2016).

60. Aubry, J., Pierlot, C., Rigaudy, J. & Schmidt, R. Reversible Binding of Oxygen to Aromatic Compounds. *Acc. Chem. Res.* **36**, 668–675 (2003).

61. Sharma, S. & Kakade, N. Dose enhancement in gold nanoparticle-aided radiotherapy for the therapeutic photon beams using Monte Carlo technique. *J. Cancer Res. Ther.* **11**, 94 (2015).

62. Guidelli, E. J., Ramos, A. P. & Baffa, O. Unconventional Increase in Non-Radiative Transitions in Plasmon-Enhanced Luminescence: A Distance-Dependent Coupling. *Sci. Rep.* **6**, (2016).

63. Kang, P. *et al.* A novel sonication route to prepare anthracene nanoparticles. *Mater. Res. Bull.* **39**, 545–551 (2004).

64. Guidelli, E. J., Ramos, A. P., Zaniquelli, M. E. D., Nicolucci, P. & Baffa, O. Synthesis and characterization of silver/alanine nanocomposites for radiation detection in medical applications: the influence of particle size on the detection properties. *Nanoscale* **4**, 2884–93 (2012).

65. Jeong, M. S. *et al.* Methodological considerations of electron spin resonance spin trapping techniques for measuring reactive oxygen species generated from metal oxide nanomaterials. *Sci. Rep.* **6**, (2016).

66. Photooxidation of anthracene under visible light with metallocarboxyphenylporphyrins. http://www.scielo.org.co/scielo.php?script=sci_arttext&pid=S0120-62302014000400021.

67. Xu, H., Zeiger, B. W. & Suslick, K. S. Sonochemical synthesis of nanomaterials. *Chem. Soc. Rev.* **42**, 2555–2567 (2013).

68. Guidelli, E. J.1. Guidelli, E. J., Baffa, O. & Clarke, D. R. Enhanced UV Emission from Silver/ZnO and Gold/ZnO Core-Shell Nanoparticles: Photoluminescence, Radioluminescence, and Optically Stimulated Luminescence. Sci. Rep. 5, (2015)., Baffa, O. & Clarke, D. R. Enhanced UV Emission from Silver/ZnO and Gold/ZnO Core-Shell Nanoparticles: Photoluminescence, Radioluminescence, and Optically Stimulated Luminescence. *Sci. Rep.* **5**, (2015).

69. Fratoddi, I. *et al.* Core shell hybrids based on noble metal nanoparticles and conjugated polymers: Synthesis and characterization. *Nanoscale Res. Lett.* **6**, 98 (2011).

70. Chen, D., Shi, J. & Shen, H. High-dispersed catalysts of core–shell structured Au@SiO2 for formaldehyde catalytic oxidation. *Chem. Eng. J.* **385**, 123887 (2020).

71. Keuren, E. Van, Georgieva, E. & Durst, M. Kinetics of the Growth of Anthracene Nanoparticles. *J. Dispers. Sci. Technol.* **24**, 721–729 (2003).

72. Xu, M. *et al.* Synthesis and comparative biological properties of Ag-PEG nanoparticles with tunable morphologies from Janus to multi-core shell structure. *Materials (Basel).* **11**, (2018).

73. Guidelli, E. J., Baffa, O. & Clarke, D. R. Enhanced UV Emission from Silver/ZnO and Gold/ZnO Core-Shell Nanoparticles: Photoluminescence, Radioluminescence, and Optically Stimulated Luminescence. *Sci. Rep.* **5**, 1–11 (2015).

74. Kao, S., Asanov, A. N. & Oldham, P. B. A comparison of fluorescence inner-filter effects for different cell configurations. *Instrumentation Science and Technology* vol. 26 375–387 (1998).

75. Yeshchenko, O. A., Kondratenko, S. V. & Kozachenko, V. V. Surface plasmon enhanced photoluminescence from fullerene C 60 film on Au nanoparticles array: Resonant dependence on excitation frequency. *J. Appl. Phys.* **111**, (2012).

76. Finkelmeier, N. *SYNTHESIS AND FLUORESCENCE PROPERTIES OF ANTHRACENE DERIVATIVES AND THEIR METAL COMPLEXES.*

77. Su, K. H. *et al.* Interparticle coupling effects on plasmon resonances of nanogold particles. *Nano Lett.* **3**, 1087–1090 (2003).

78. Peter, M. *et al.* Fluorescence enhancement by a dark plasmon mode. *Appl. Phys. B Lasers Opt.* **124**, 0 (2018).

79. Ray, K., Badugu, R. & Lakowicz, J. R. Distance-dependent metal-enhanced fluorescence from Langmuir-Blodgett monolayers of alkyl-NBD derivatives on silver island films. *Langmuir* **22**, 8374–8 (2006).

80. Camposeo, A. *et al.* Metal-Enhanced Near-Infrared Fluorescence by Micropatterned Gold Nanocages. *ACS Nano* **9**, 10047–10054 (2015).

81. Szmacinski, H., Badugu, R. & Lakowicz, J. R. Fabrication and Characterization of Planar Plasmonic Substrates with High Fluorescence Enhancement. *J. Phys. Chem. C. Nanomater. Interfaces* **114**, 21142–21149 (2010).

82. Clement, S., Deng, W., Camilleri, E., Wilson, B. C. & Goldys, E. M. X-ray induced singlet oxygen generation by nanoparticle-photosensitizer conjugates for photodynamic therapy: Determination of singlet oxygen quantum yield. *Sci. Rep.* **6**, (2016).

83. Nakamura, K. *et al.* Reevaluation of analytical methods for photogenerated singlet oxygen. *J. Clin. Biochem. Nutr.* **49**, 87–95 (2011).

84. Mangkhalathon, A., Teerakapong, A., Morales, N. P., Morkmued, S. & Damrongrungruang, T. Singlet oxygen formation in photodynamic therapy using guaiazulene and red laser: an in vitro study. in 322 (SPIE-Intl Soc Optical Eng, 2019). doi:10.1117/12.2525414.

85. Kolemen, S. *et al.* Remote-Controlled Release of Singlet Oxygen by the Plasmonic Heating of Endoperoxide-Modified Gold Nanorods: Towards a Paradigm Change in Photodynamic Therapy. *Angew. Chemie - Int. Ed.* **55**, 3606–3610 (2016).

86. Díaz-Uribe C. E. , Vallejo-Lozada W. A., O. F. M. Photooxidation of anthracene under visible light with metallocarboxyphenylporphyrins. *Rev. Fac. Ing. Univ. Antioquia* 225–230 (2014).

87. Martins, S., Farinha, J. P. S., Baleizã, C. & Berberan-Santos, M. N. Controlled release of singlet oxygen using diphenylanthracene functionalized polymer nanoparticles † ChemComm COMMUNICATION. (2014) doi:10.1039/c3cc48293f.

88. Fudickar, W. & Linker, T. Synthesis of Pyridylanthracenes and Their Reversible Reaction with Singlet Oxygen to Endoperoxides. *J. Org. Chem.* **82**, 9258–9262 (2017).

89. Martins, S., Farinha, J. P. S., Baleizão, C. & Berberan-Santos, M. N. Controlled release of singlet oxygen using diphenylanthracene functionalized polymer nanoparticles. *Chem. Commun.* **50**, 3317–3320 (2014).

90. Liu, H., Carter, P. J. H., Laan, A. C., Eelkema, R. & Denkova, A. G. Singlet Oxygen Sensor Green is not a Suitable Probe for 1O2 in the Presence of Ionizing Radiation. *Sci. Rep.* **9**, (2019).

91. Matsumura, Y. *et al.* Detection of high-frequency ultrasound-induced singlet oxygen by the ESR spin-trapping method. *Chem. Lett.* **42**, 1291–1293 (2013).

92. Hubenko, K. *et al.* Reactive oxygen species generation in aqueous solutions containing GdVO4:Eu3+ nanoparticles and their complexes with methylene blue. *Nanoscale Res. Lett.* **13**, 100 (2018).

93. Martins, S., Farinha, J. P. S., Baleizã, C. & Berberan-Santos, M. N. Controlled release of singlet oxygen using diphenylanthracene functionalized polymer nanoparticles † ChemComm COMMUNICATION. (2014) doi:10.1039/c3cc48293f.

94. Behrouzkia, Z., Zohdiaghdam, R., Khalkhali, H. R. & Mousavi, F. Evaluation of Gold Nanoparticle Size Effect on Dose Enhancement Factor in Megavoltage Beam Radiotherapy Using MAGICA Polymer Gel Dosimeter. *J. Biomed. Phys. Eng.* **9**, 89–96 (2019).